ACS NANO

www.acsnano.org

ARTICLE

An Ionizable Lipid Material with a Vitamin E Scaffold as an mRNA Vaccine Platform for Efficient Cytotoxic T Cell Responses

Ryotaro Oyama, Harumichi Ishigame, Hiroki Tanaka, Naho Tateshita, Moeko Itazawa, Ryosuke Imai, Naomasa Nishiumi, Jun-ichi Kishikawa, Takayuki Kato, Jessica Anindita, Yoshifumi Nishikawa, Masatoshi Maeki, Manabu Tokeshi, Kota Tange, Yuta Nakai, Yu Sakurai, Takaharu Okada,* and Hidetaka Akita*

Cite This: *ACS Nano* 2023, 17, 18758−18774

Read Online

ACCESS | Metrics & More | Article Recommendations | Supporting Information

ABSTRACT: RNA vaccines based on lipid nanoparticles (LNPs) with *in vitro* transcribed mRNA (IVT-mRNA) encapsulated are now a currently successful but still evolving modality of vaccines. One of the advantages of RNA vaccines is their ability to induce $CD8^+$ T-cell-mediated cellular immunity that is indispensable for excluding pathogen-infected cells or cancer cells from the body. In this study, we report on the development of LNPs with an enhanced capability for inducing cellular immunity by using an ionizable lipid with a vitamin E scaffold. An RNA vaccine that contained this ionizable lipid and an IVT-mRNA encoding a model antigen ovalbumin (OVA) induced OVA-specific cytotoxic T cell responses and showed an antitumor effect against an E.G7-OVA tumor model. Vaccination with the LNPs conferred protection against lethal infection by *Toxoplasma gondii* using its antigen TgPF. The vitamin E scaffold-dependent type I interferon response was important for effector $CD8^+$ T cell differentiation induced by the mRNA-LNPs. Our findings also revealed that conventional dendritic cells (cDCs) were essential for achieving $CD8^+$ T cell responses induced by the mRNA-LNPs, while the XCR1-positive subset of cDCs, cDC1 specialized for antigen cross-presentation, was not required. Consistently, the mRNA-LNPs were found to selectively transfect another subset of cDCs, cDC2 that had migrated from the skin to lymph nodes, where they could make vaccine-antigen-dependent contacts with $CD8^+$ T cells. The findings indicate that the activation of innate immune signaling by the adjuvant activity of the vitamin E scaffold and the expression of antigens in cDC2 are important for subsequent antigen presentation and the establishment of antigen-specific immune responses.

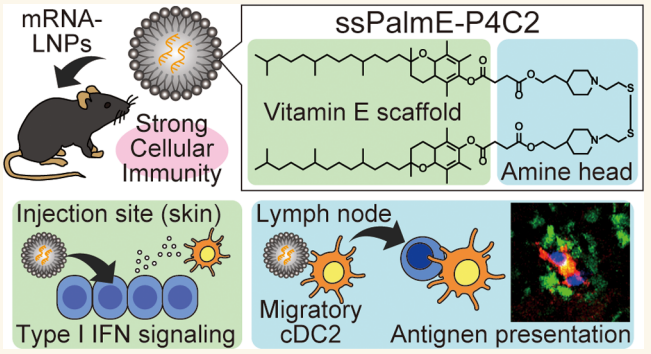

KEYWORDS: *vitamin E, RNA vaccine, adjuvant, lipid nanoparticle, cellular immunity, innate immunity*

INTRODUCTION

RNA vaccines based on *in vitro* transcribed mRNA (IVT-mRNA) are promising modality of vaccines. Since any antigen protein of interest can theoretically be introduced to our body by designing the sequence of the IVT-mRNA,[1] a large variety of diseases would be therapeutic targets. The usefulness of RNA vaccines is clearly evident from the development of vaccines against SARS-CoV-2:[2−5] clinical trials of the RNA vaccine against this virus had been started only 2 months after the determination of the viral genome sequence,[1] and vaccine efficacy in excess of 90% in Phase III trials was reported within 10 months.[2] Another advantage of the RNA vaccines is their potential to induce antigen-specific cellular immunity in which $CD8^+$ T cells play a central role in excluding infected cells and/or cells that had mutated from normal cells.[6−9] Therefore, it has been assumed that the RNA vaccine is a suitable therapeutic modality for the treatment of infections of intracellular parasitic microorganisms.[10−12] The ease of

Received: March 10, 2023
Accepted: August 17, 2023
Published: September 26, 2023

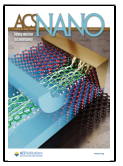

https://doi.org/10.1021/acsnano.3c02251
ACS Nano 2023, 17, 18758−18774

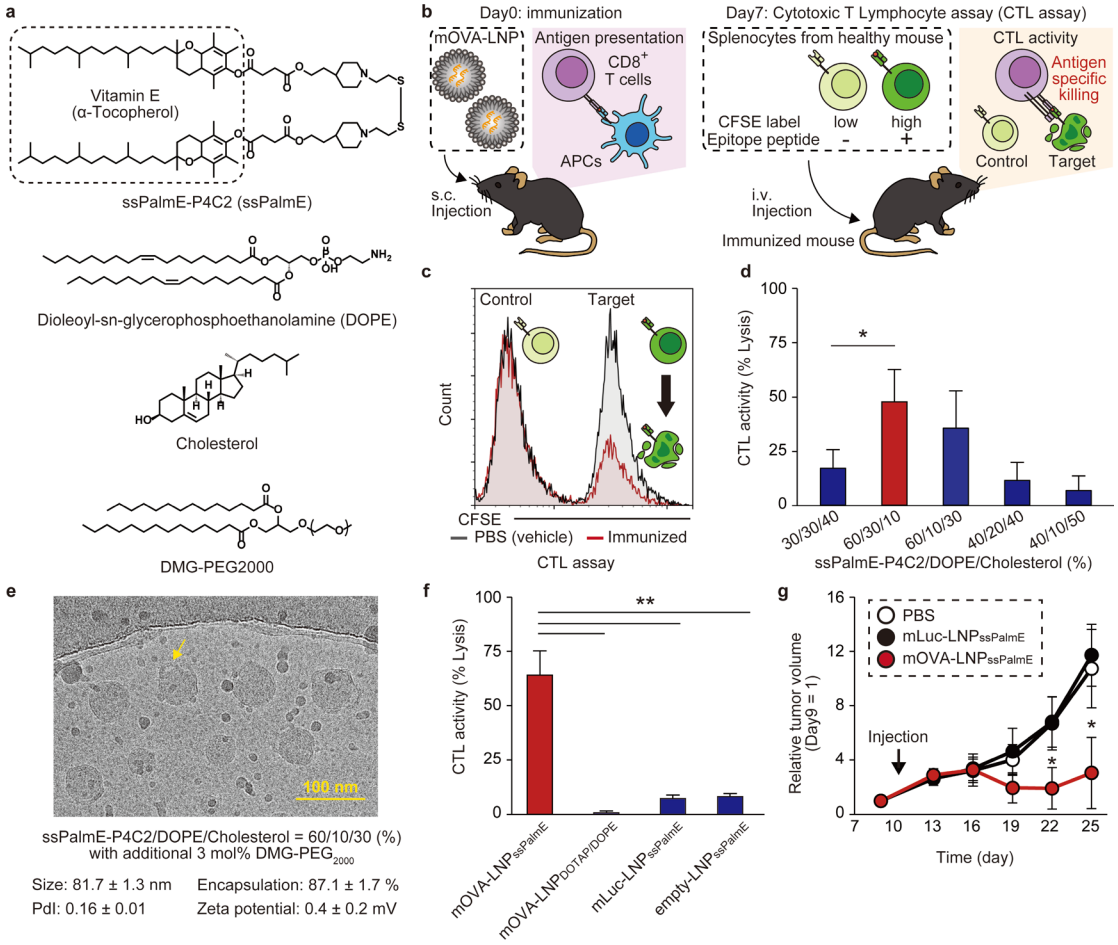

Figure 1. Antigen-specific CTL activation and antitumor effect of mRNA-LNP$_{ssPalmE}$. (a) Chemical structures of the lipids used in this study. (b) Graphical scheme of CTL assay. The activation of cytotoxic T lymphocytes was evaluated by means of a CTL assay (described in the Methods section). (c) Representative histogram of the nonimmunized mice and mRNA-LNPs (ssPalmE-P4C2/DOPE/Chol = 60/30/10)-injected mice. (d) CTL activities of the top 5 lipid compositions in each CTL assay (Figure S3a). (e) Cryo-EM image and property of particles of the mRNA-LNP$_{ssPalmE}$. Bar indicates 100 nm. Bleb structures are indicated in yellow. (f) Comparison of CTL activity to control samples. (g) Therapeutic antitumor effect of the mRNA-LNP$_{ssPalmE}$. E.G7-OVA inoculated mice were immunized with mOVA-LNP$_{ssPalmE}$ or mLuc-LNP$_{ssPalmE}$, and their tumor size was then monitored. *; $p < 0.05$ and **; $p < 0.01$.

designing and efficient activation of cellular immunity also makes the RNA vaccine a suitable modality for developing a personalized cancer vaccine using the patient's own genetic information on neo-antigens.[13−17]

Since IVT-mRNA is vulnerable to enzymatic degradation, drug delivery systems (DDS) that protect it are needed for successful *in vivo* applications. One of the most promising DDS are lipid nanoparticles (LNPs) which contain ionizable lipids as key components. An important functional unit of the ionizable lipid is a pH-responsive tertiary amine group that can develop a cationic charge only in an acidic environment. While the LNPs avoid nonspecific electrostatic interactions with biomolecules under physiological conditions, they can efficiently interact with the anionic endosomal membrane during the acidification of endosomes and can facilitate the delivery of the IVT-mRNA to the cytoplasm.[1,18] The IVT-mRNA is then translated to the encoded proteins by the ribosomes in the cytoplasm.

For the activation of antigen-specific immune responses, the activation of innate immunity, as well as the production of an antigen protein, is a prerequisite.[19−22] It has been hypothesized that one possible component that stimulates innate immunity is the ionizable lipid in LNPs.[19,22,23] This hypothesis has been confirmed from the viewpoint of the induction of humoral immunity. Alameh et al. showed that the co-injection of LNPs with antigen proteins induced the production of antigen-specific antibodies regardless of the presence or absence of encapsulated IVT-mRNA.[22] When the antigen proteins were injected with LNPs that contained no ionizable lipids, the production of antigen-specific antibodies was not observed. It therefore appears that ionizable lipids could be key molecules for both antigen production and innate immune signaling, although the mechanism responsible for immune activation has not been completely clarified.

Inspired by these observations, we assumed that the modification of the chemical structure of ionizable lipids from the viewpoint of the activation of cellular immunity represents a possible strategy for the further improvement of mRNA-LNPs vaccines against parasite infections and/or cancer. We previously demonstrated that the modification of the hydrophobic scaffold of ionizable lipids conferred specific physiological functions to these molecules.[24,25] An unexpected observation was that an ionizable lipid containing vitamin E scaffolds showed an efficient activation of cellular immunity when the LNPs contained a plasmid DNA.[26,27] An ionizable lipid with vitamin E scaffolds could also be used for preparing

https://doi.org/10.1021/acsnano.3c02251
ACS Nano 2023, 17, 18758−18774

RNA-introduced *ex vivo* dendritic cells (DCs) vaccines for cancers when combined with a fusogenic KALA peptide.[28] However, the issue of how the activation of innate immunity, which is preferable for cellular immunity, is induced by the vitamin E scaffold and whether this strategy could be applicable to a directly injectable RNA vaccine for *in vivo* use remains unclear.

In this study, we investigated the issue of whether the use of mRNA-LNPs containing an ionizable lipid with a vitamin E scaffold could induce strong activation of cellular immunity against an antigen protein encoded in the IVT-mRNA. The mechanisms responsible for the vaccine activity were also investigated from the viewpoints of innate immune signaling and identification of subpopulations of antigen-presenting cells (APCs).

RESULTS

Development of RNA Vaccine for Cellular Immunity.

The aim of this study was to develop an RNA vaccine specific for activating cellular immunity and to investigate the mechanism of action of the process. An ionizable lipid with a vitamin E scaffold (SS-cleavable and pH-activated lipid-like material (ssPalmE-P4C2, Figure 1a) was used as the ionizable lipid.[29] The suffix P4C2 denotes a piperidine moiety in the tertiary amine heads that serves to enhance the efficiency of endosomal escape.[30] After the endosomal escape, the IVT-mRNA is released from the LNPs to be translated into a protein.[31] The ssPalm contains a disulfide bond in its structure, the function of which is to enhance the intracellular release of the IVT-mRNA.[28,29]

The mRNA-LNPs containing ssPalmE-P4C2 (mRNA-LNP$_{ssPalmE}$) are stabilized with dioleoyl-*sn*-glycero phosphatidyl ethanolamine (DOPE) and cholesterol. A lipid-conjugated poly(ethylene glycol) (DMG-PEG$_{2000}$) was also added to suppress aggregation. An initial screening of the lipid compositions was performed. The mRNA-LNPs used in the screening were prepared by the ethanol dilution method by vortex mixing. An ethanol solution containing ssPalmE-P4C2, DOPE, cholesterol, and DMG-PEG$_{2000}$ was mixed with an IVT-mRNA solution to form the mRNA-LNP$_{ssPalmE}$. The external buffer containing ethanol was then replaced with phosphate buffered saline (PBS (−)) by ultrafiltration. The procedure used in the screening is shown in Figure S1. Forty-three lipid compositions that contained more than 10% ssPalmE-P4C2 and less than 50% cholesterol were tested. All of the lipid compositions contained an additional 3 mol% DMG-PEG$_{2000}$ of total lipid. Information concerning the properties of the 43 LNPs was then obtained. This series of mRNA-LNP$_{ssPalmE}$ showed encapsulation efficiencies ranging from 0 to 91%, particle sizes ranging from 99 to 167 nm, PdI ranging from 0.074 to 0.229, and zeta potential ranging from −10.7 to −2.3 mV (Figure S2a). A high encapsulation efficiency was observed in the region where the ssPalm content was >20% and with a DOPE content of less than 40% (Figure S2b). Particle size tended to be smaller with a higher cholesterol content (Figure S2c). An ssPalmE content lower than 20% resulted in a large PdI, indicating the formation of heterogeneous particles. From these 43 lipid compositions, 26 samples with an encapsulation efficiency in excess of 50% were selected for further investigation. The efficacy of mRNA-LNP$_{ssPalmE}$ as an RNA vaccine for activating cellular immunity was evaluated by a Cytotoxic T lymphocyte assay (CTL assay). The IVT-mRNA encoding model antigen Ovalbumin (OVA) was encapsulated in the LNPs (mOVA-LNP$_{ssPalmE}$), and subcutaneously administrated. At 1 week after the administration, the activation of cellular immunity was evaluated by measuring the epitope peptide-specific lysis of the cells (Figure 1b, Figure 1c, see the Methods section for details). The results of the CTL assay are summarized in Figures S3a, S3b. The mRNA-LNP$_{ssPalmE}$ with the lipid composition of ssPalmE-P4C2/DOPE/cholesterol = 30/30/40 was used as a control particle. Comparison of the relative CTL activity indicated that mRNA-LNPs that contained 40−80% ssPalm had CTL activity superior to that of the control mRNA-LNPs (Figure S3c). No correlation was found between CTL activity and the properties of the particles such as size, PdI, zeta-potential, and encapsulation efficiency. (Figure S3d). Comparison of the top-performing LNPs in each CTL assay revealed that ssPalmE-P4C2/DOPE/cholesterol = 60/30/10 with an additional 3 mol% of DMG-PEG$_{2000}$ showed the highest CTL activity (Figure 1d).

The mRNA-LNP$_{ssPalmE}$ was then prepared using an iLiNP microfluidic device (Figure S4a).[32] The effect of the flow rate ratio (FRR) of the IVT-mRNA solution and lipid solution and the ratio of lipids (nmol) to IVT-mRNA (μg) (L/R ratio) were investigated. The results indicated that FRR 1.5 is the preferred condition (Figure S4b). An FRR lower than 1.0 impaired the mRNA-LNPs formation and resulted in aggregation or failure to encapsulate the IVT-mRNA, while a higher FRR above 3.0 resulted in heterogeneous mRNA-LNPs with PdI values in excess of 0.2. Therefore, the FRR was fixed at 1.5 for subsequent investigations. The L/R ratio from 14.6 to 394.5, which corresponds to an N/P ratio from 6.0 to 161.1 (the ssPalmE-P4C2 contains two amine moieties in one molecule), had no effect on the particle formation at FRR above 1.5.

In the case of intramuscular administration, the activation of humoral immunity was dependent on the size of the mRNA-LNPs.[33] To evaluate the effects of size on the activation of cellular immunity, the conditions for preparing stable, larger-sized LNPs (>100 nm) were explored by changing the total flow rate of the solutions and the concentration of NaCl in the buffers containing IVT-mRNA. Particle size tended to increase at high salt concentrations when the L/R ratio was 14.6 and 43.8, while the encapsulation efficiency decreased. The encapsulation efficiency was significantly impaired even at higher L/R ratios (43.8) when the NaCl concentration was increased to 750 mM. In the presence of 150 mM NaCl, the decrease in the total flow rate resulted in an increased size without any impairment of encapsulation. mRNA-LNPs with different L/R ratios, the sizes of which ranged from approximately 140−160 nm, were used for immunization. The optimum L/R ratio was found to be 131.5 (Figure S4e,f). Finally, the CTL activity of the mRNA-LNP$_{ssPalmE}$ with particle sizes of 70 or 164 nm was compared at an L/R ratio of 131.5. As a result, it was found that a smaller mRNA-LNP$_{ssPalmE}$ was preferred in terms of activating cellular immunity (Figure S4g,h). It was therefore concluded that the mRNA-LNP$_{ssPalmE}$ with a size of 70 nm was the optimal formulation.

The properties of the mRNA-LNP$_{ssPalmE}$ particles and Cryo-EM images are shown (Figure 1e, additional original images are shown in Figure S5). The mRNA-LNP$_{ssPalmE}$ had a spherical shape. Some of the particles showed bleb-like structures (indicated by yellow in Figure 1e, Figure S5) with an interior aqueous phase.[34] The size of the particles was

https://doi.org/10.1021/acsnano.3c02251
ACS Nano 2023, 17, 18758−18774

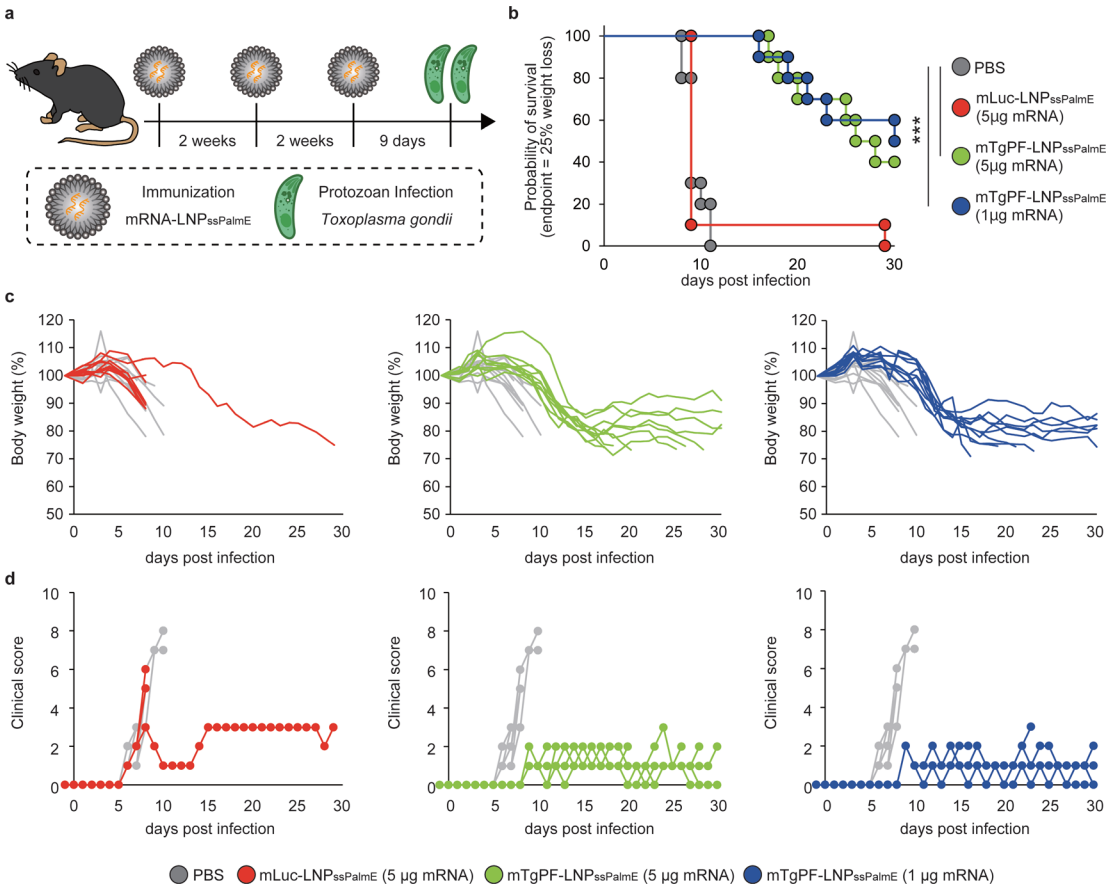

Figure 2. Antiprotozoan effect of the mRNA-LNP$_{ssPalmE}$. (a) Schematic illustration of the infection experiment with *Toxoplasma gondii*. (b–d) Prophylactic effects of mTgPF-LNP$_{ssPalmE}$. Mice were immunized with mLuc-LNP$_{ssPalmE}$, mTgPF-LNP$_{ssPalmE}$ (5.0 μg mRNA), or mTgPF-LNP$_{ssPalmE}$ (1.0 μg mRNA) once every 2 weeks for 3 times. Mice were then infected with *Toxoplasma gondii* 9 days after the third immunization, and their condition was then monitored. (b) Survival rate using the Kaplan–Meier method. End point was when the body weight has decreased more than 25% of Day − 1 (n = 10, *; p < 0.001). (c) Body weight and (d) clinical score are shown.**

below 100 nm, which is consistent with the dynamic light scattering results.

The mRNA-LNP$_{ssPalmE}$ equivalent to 0.05 μg OVA mRNA induced a higher OVA-specific CTL activity than a conventional cationic mRNA vector using 1,2-dioleoyl-3-trimethylammonium-propane (DOTAP) (Figure 1f).[35] Consistent with the strong activation of cellular immunity, the mOVA-LNP$_{ssPalmE}$ showed antitumor activity against a tumor model expressing this antigen (E.G7-OVA) in the therapeutic regimen (Figure 1g). The preventive antitumor activity for human antigens was investigated using human NY-ESO-1 (hNY-ESO-1). At 7 days after vaccinating mice with mhNY-ESO-1-LNP$_{ssPalmE}$, they were inoculated with CT26 cells expressing hNY-ESO-1 (Figure S6). As a result, the mice that had been immunized with mhNY-ESO-1-LNP$_{ssPalmE}$ showed significant tumor growth inhibition, while no preventative effect was detected in the mice that had been immunized with the mOVA-LNP$_{ssPalmE}$. These observations indicate that mRNA-LNP$_{ssPalmE}$ can be used as a cancer vaccine.

Changes in body weight after injections were below 10% in both s.c. injection and i.m. injection (Figure S7a). Three repeated i.m. administrations of the mOVA-LNP$_{ssPalmE}$ showed no increase in hepatic injury markers (Figure S7b, c). At over a week after an s.c. injection of the LNP$_{ssPalmE}$, no grossly visible tissue damage around the injection site was observed. At 7 days after an s.c. injection of the LNP$_{ssPalmE}$, the anatomical structure of the skin at the injection site was not noticeably disrupted although the epidermis had moderately thickened and the number of nuclei in the dermal parenchyma appeared to be moderately increased (Figure S8). Therefore, it would appear that mRNA-LNP$_{ssPalmE}$ has low systemic toxicity. These observations suggest that mRNA-LNP$_{ssPalmE}$ is a suitable carrier for activating antigen-specific cellular immunity.

Prophylactic Antiprotozoan Effect. The prophylactic antiprotozoan effect against *Toxoplasma gondii* was evaluated using *Toxoplasma gondii* profilin (TgPF) as the target antigen. Naïve mice were administered with mTgPF-LNP$_{ssPalmE}$ once every 2 weeks for 3 times. They were then challenged with an infection of *Toxoplasma gondii* 9 days after the last administration, and the survival rate, body weight, and clinical score were evaluated (Figure 2a). Both a low dose (1 μg mRNA) and a high dose (5 μg mRNA) regimen elicited prophylactic antiprotozoan activity in an encoded protein-dependent manner (Figure 2b–d). These observations suggest that the ionizable lipid with the vitamin E scaffolds has the ability to induce cellular immunity against parasitic infection and cancers.

mRNA-LNP$_{ssPalmE}$ Induces Antigen-Specific CD8$^+$ T Cell Proliferation and Differentiation. To track the *in vivo* antigen-specific CD8$^+$ T cell response to mRNA-LNP$_{ssPalmE}$, we performed an adoptive transfer of CD8$^+$ T cells from OT-I

https://doi.org/10.1021/acsnano.3c02251
ACS Nano 2023, 17, 18758–18774

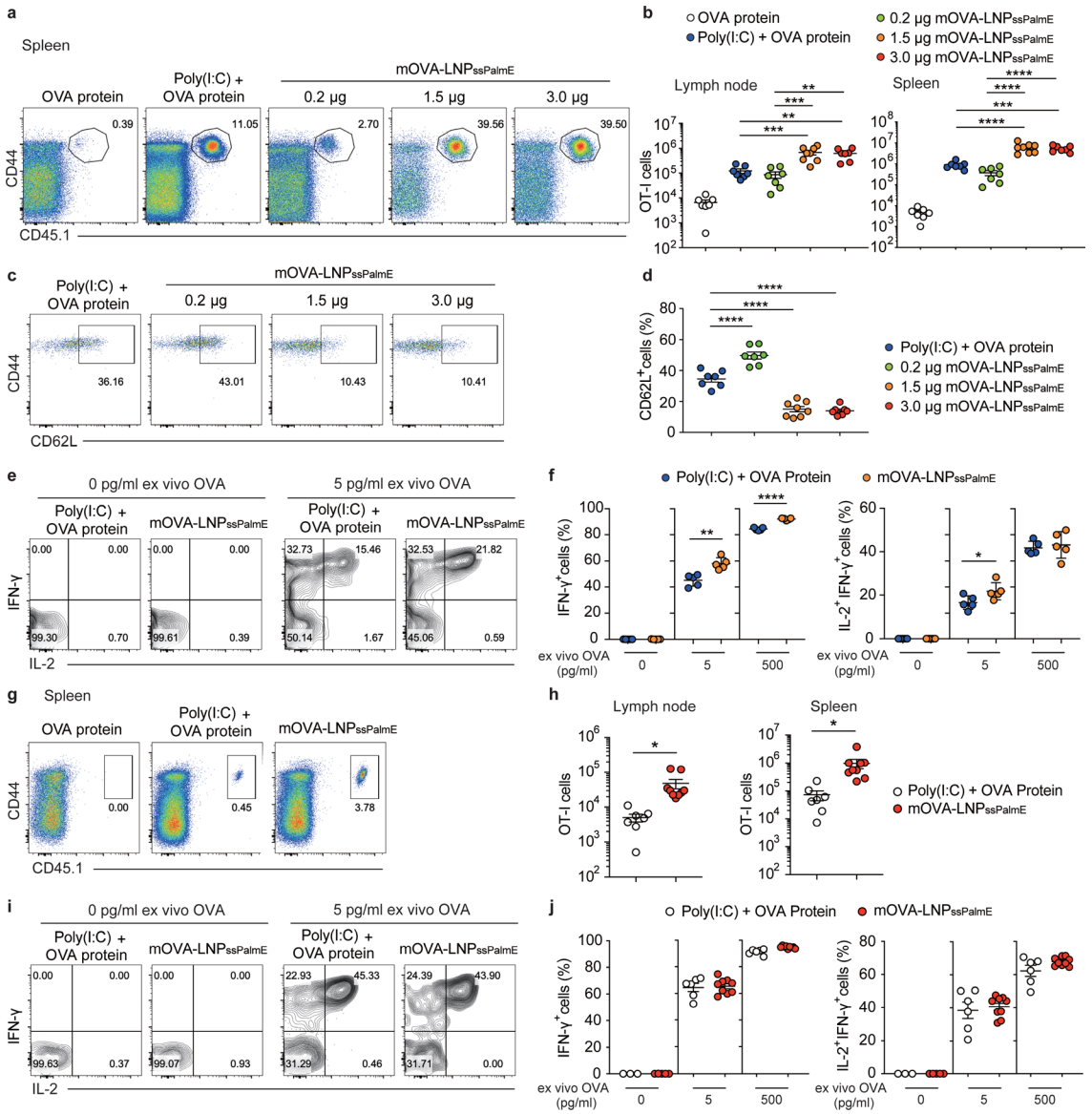

Figure 3. Antigen-dependent expansion of CD8$^+$ T cells and their differentiation to effector and memory CTLs by mRNA-LNP$_{ssPalmE}$. (a−d) Antigen-dependent expansion and differentiation to effector cells of CD8$^+$ T cells. OT-I CD8$^+$ T cells were transferred into congenic recipient mice that were subsequently immunized with poly(I:C) plus soluble OVA protein or the indicated dose of mOVA-LNP$_{ssPalmE}$, and analyzed by flow cytometry on day 7 after immunization. (a) Representative flow cytometry plots of transferred OT-I CD8$^+$ T cells in the spleen, (b) number of transferred OT-I CD8$^+$ T cells in the draining lymph nodes and spleen, (c) flow cytometry plot, and (d) percentage of CD62L$^+$ cells in the total OT-I CD8$^+$ T cell population in the spleen are shown. (e, f) *Ex vivo* stimulation of the splenocytes from immunized mice. At 7 days after immunization, the splenocytes were stimulated with the OVA (257−264) peptide for 5 h *in vitro*. (e) Representative flow cytometry plots and (f) percentage of OT-I CD8$^+$ T cells producing IFN-γ and IL-2 cells are shown. (g,j) Differentiation to effector cells of CD8$^+$ T cells. OT-I CD8$^+$ T cells were transferred into congenic recipient mice that were subsequently immunized with poly(I:C) plus soluble OVA protein or mOVA-LNP$_{ssPalmE}$, and analyzed by flow cytometry on day 35 after immunization. (g) Representative flow cytometry plots and (h) numbers of transferred OT-I CD8$^+$ T cells in the draining lymph nodes and spleen on day 35 after immunization. (i) Representative flow cytometry plots and (j) percentage of OT-I CD8$^+$ T cells producing IFN-γ and IL-2 in the spleen on day 35 after immunization following stimulation with OVA (257−264) peptide for 5 h *in vitro* are shown. The mean ± s.e. is shown by the bars together with the symbols representing the individual data. (b, d, h, j) Data are pooled from 2 to 4 independent experiments. (f) Data are representative of two independent experiments. **; $p < 0.01$, *; $p < 0.001$ and ****; $p < 0.0001$.**

TCR transgenic mice into wild-type mice. The recipient mice were then subcutaneously immunized at the base of the tail with the OVA protein alone, the OVA protein plus Poly(I:C), or various doses of mOVA-LNP$_{ssPalmE}$. The number of OT-I CD8$^+$ T cells that proliferated in the draining lymph nodes (inguinal lymph node) or spleen at 7 days after immunization was much larger when the mice were immunized with the mOVA-LNP$_{ssPalmE}$ containing 1.5 or 3.0 μg of mRNA compared to mice that were immunized with mOVA-LNP$_{ssPalmE}$ containing 0.2 μg of mRNA or with the OVA protein plus poly(I:C) (Figure 3a,b). Accordingly, the greatest downregulation of CD62L$^+$ of OT-I CD8$^+$ T cells for differentiating to effector T cells was induced by the mOVA-LNP$_{ssPalmE}$ containing 1.5 or 3.0 μg of mRNA (Figure 3c,d). In addition, the mOVA-LNP$_{ssPalmE}$ containing 1.5 μg of mRNA induced significantly more IFN-γ-producing OT-I CD8$^+$ T

https://doi.org/10.1021/acsnano.3c02251
ACS Nano 2023, 17, 18758−18774

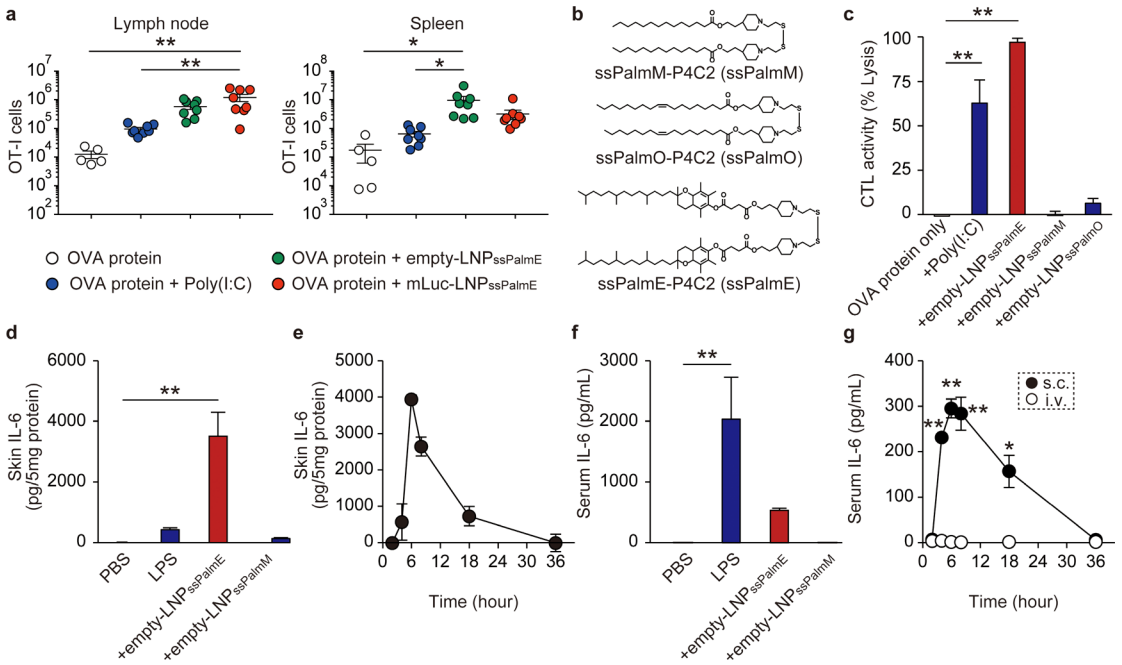

Figure 4. Adjuvant activity of vitamin E scaffolds. (a) Adjuvant activities of mRNA-LNP$_{ssPalmE}$ and empty-LNP$_{ssPalmE}$. OT-I CD8$^+$ T cells were transferred into congenic recipient mice that were subsequently injected with soluble OVA protein alone or in combination with poly(I:C), empty-LNP$_{ssPalmE}$, or mLuc-LNP$_{ssPalmE}$, and analyzed by flow cytometry on day 7 after immunization. The number of transferred OT-I CD8$^+$ T cells in the draining lymph nodes and spleen is shown. (b) Chemical structures of ssPalmM-P4C2, ssPalmO-P4C2, and ssPalmE-P4C2. (c) CTL activity of the mice immunized by the co-injection of the OVA protein and empty-LNP$_{ssPalmM}$, empty-LNP$_{ssPalmO}$, or empty-LNP$_{ssPalmE}$. Mice were subcutaneously immunized with the OVA protein and Poly(I:C), the OVA protein and empty-LNP$_{ssPalmE}$, the OVA protein and empty-LNP$_{ssPalmM}$, or the OVA protein and empty-LNP$_{ssPalmO}$. (d-g) IL-6 production by LNP$_{ssPalmE}$ injection. Mice were subcutaneously injected with empty-LNP$_{ssPalmE}$, empty-LNP$_{ssPalmM}$, or LPS. Skin tissues at the injected site (1.5 cm square) were collected, and whole protein was extracted. In parallel, blood samples were collected, and serum was extracted. The IL-6 concentration in the extract from skin tissue (d) 6 h after the injection and (e) 2, 4, 6, 8, 18, and 36 h after the injection of empty-LNP$_{ssPalmE}$. IL-6 concentration in the serum (f) 6 h after the injection and (g) 2, 4, 6, 8, 18, and 36 h after the empty-LNP$_{ssPalmE}$ injection compared to the intravenous empty-LNP$_{ssPalmE}$ injection. (a) Mean ± s.e. is shown by the bars together with the symbols representing the individual data. Data are pooled from two independent experiments. (c, d, f, g) Mean ± s.e. are shown. *; $p < 0.05$ and **; $p < 0.01$.

cells than did the OVA protein plus poly(I:C) (Figure 3e,f). These results confirm that the mOVA-LNP$_{ssPalmE}$ strongly drives antigen-specific CD8$^+$ T cell proliferation and differentiation to effector cells.

mOVA-LNP$_{ssPalmE}$ Induces Memory CD8$^+$ T Cells. We then analyzed the number of memory OT-I CD8$^+$ T cells 5 weeks after immunization (Figure 3g,h). The findings indicated that more antigen-engaged OT-I CD8$^+$ T cells were sustained in mice that had been immunized with mOVA-LNP$_{ssPalmE}$ containing 1.5 μg of mRNA than in mice that had been immunized with the OVA protein plus poly(I:C). In the memory phase, these OT-I CD8$^+$ T cells efficiently produced IL-2 and IFN-γ when restimulated *in vitro* with the OVA (257−264) peptide (Figure 3i,j). These results indicate that mOVA-LNP$_{ssPalmE}$ robustly induces antigen-specific memory CD8$^+$ T cells.

Adjuvant Activity of the LNP$_{ssPalmE}$. The efficient induction of effector and memory CD8$^+$ T cells suggests that the injection of mRNA-LNP$_{ssPalmE}$ stimulated both the production of antigen proteins and the activation of innate immunity. To clarify the mechanism responsible for the activation of innate immunity, empty-LNP$_{ssPalmE}$ or LNPs containing IVT-mRNA of luciferase (mLuc-LNP$_{ssPalmE}$) were coadministered subcutaneously with the OVA protein to mice that had been inoculated with OT-I CD8$^+$ T cells. At 1 week after the immunization, the level of OT-I CD8$^+$ T cell proliferation was comparable in these groups. This result suggests that the activation of innate immunity by the LNP$_{ssPalmE}$ was probably due to the adjuvant activity of the LNP$_{ssPalmE}$ *per se*, and not by the IVT-mRNA that was encapsulated within it (Figure 4a). To further clarify the importance of the structural unit in ssPalmE-P4C2, the contribution of the scaffolds was compared by using a myristic acid-scaffold (ssPalmM-P4C2) and an oleic acid-scaffold (ssPalmO-P4C2) (Figure 4b). Empty-LNPs prepared using each ssPalm were mixed with OVA protein, and the mixtures were administered subcutaneously. As a result, only the empty-LNP$_{ssPalmE}$ induced the OVA-specific CTL activity (Figure 4c). An investigation of 13 cytokines/chemokines in serum revealed that the concentration of IL-6, KC, MCP1, and IP-10 was significantly increased at 6 h after the administration of the empty-LNP$_{ssPalmE}$ (Figure S9). The production of these chemokines is consistent with the moderately increased nuclei in the dermal parenchyma at the injection site of the empty-LNP$_{ssPalmE}$ (Figure S8) since they are involved in the recruitment of monocytes and neutrophils. These results suggest that the ssPalmE actually has adjuvant activity.

The activation of innate immunity by empty-LNP$_{ssPalmE}$ at the injection site was then examined. The production of IL-6 was used as an index for adjuvant activity since the injection of empty-LNP$_{ssPalmE}$ caused a significant increase in serum (Figure S9). The empty-LNP$_{ssPalmE}$ was administered subcutaneously, and the protein was extracted from the skin tissue at the injection site. A higher level of IL-6 was detected in the

https://doi.org/10.1021/acsnano.3c02251
ACS Nano 2023, 17, 18758−18774

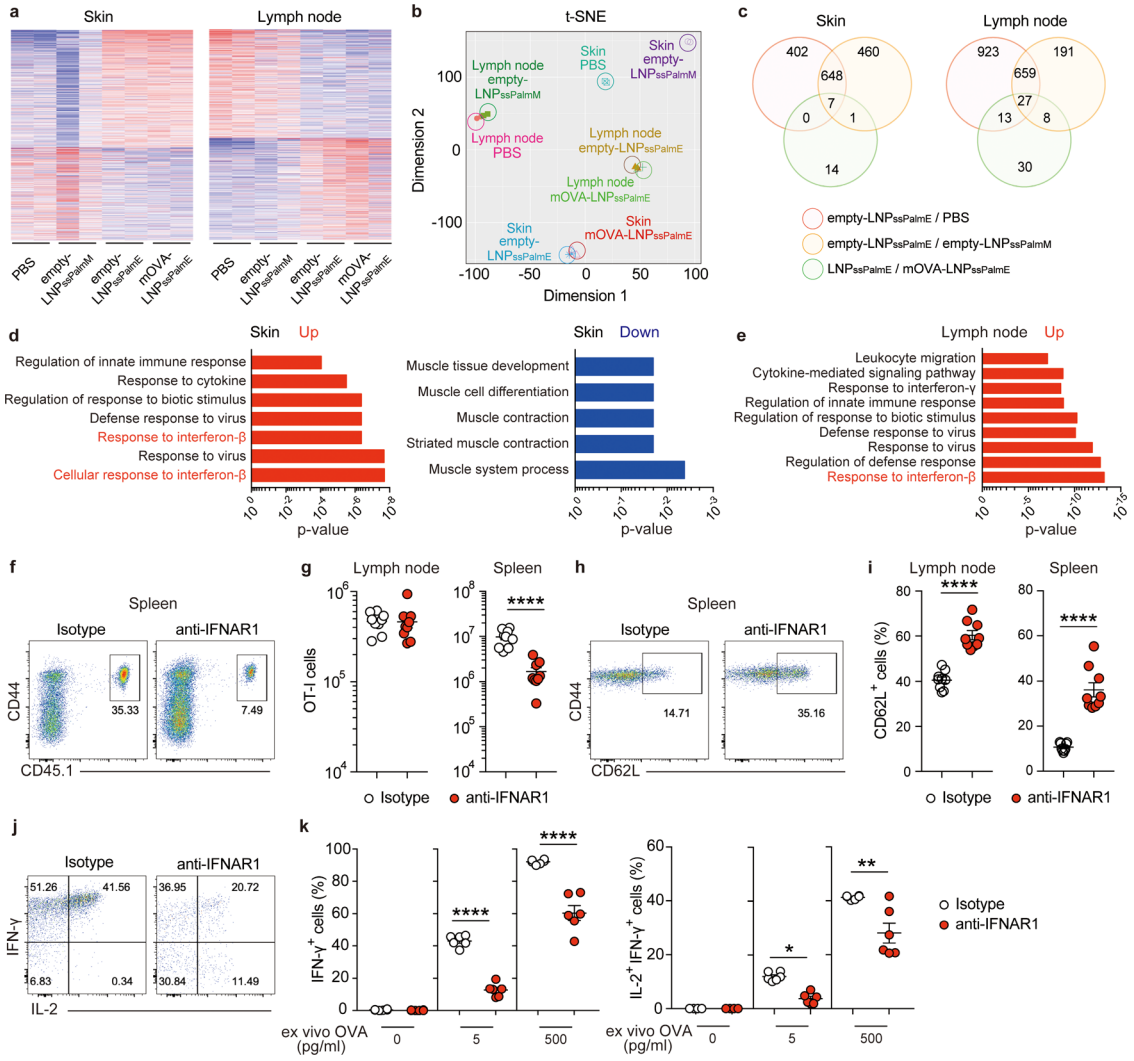

Figure 5. Contribution of type I interferon signaling to effector differentiation of CD8$^+$ T cells induced by the mRNA-LNP$_{ssPalmE}$. (a–e) RNA-sequence analysis of the skin and lymph nodes. Mice were injected s.c. with PBS, empty-LNP$_{ssPalmM}$, empty-LNP$_{ssPalmE}$, or mOVA-LNP$_{ssPalmE}$ and the skin and lymph node samples were prepared for RNA-seq analysis 1 day later. (a) Heatmap of k-means clustering, (b) t-SNE plots of RNA-seq samples, (c) Venn-diagram depicting DEGs for each treatment compared with immunization with the empty-LNP$_{ssPalmE}$, (d) the enriched pathway analysis of DEGs based on GO terms for biological processes in the skin, and (e) lymph node were shown. GAGE was used to identify increased (red) or downregulated (blue) enrichment pathways between PBS and empty-LNP$_{ssPalmE}$. (f–k) Effects of blockade of type I interferon signaling. OT-I CD8$^+$ T cells were transferred into congenic recipient mice, which were subsequently immunized with mOVA-LNP$_{ssPalmE}$. The mice were treated with an anti-IFNAR-1 antibody or isotype control antibody 1 day prior to immunization. (f) Representative flow cytometry plots of transferred OT-I CD8$^+$ T cells in the spleen, (g) number of transferred OT-I CD8$^+$ T cells in the draining lymph nodes and spleen. (h) Flow cytometry and (i) percentage of CD62L$^+$ cells in the total OT-I CD8$^+$ T cell population in the draining lymph nodes and spleen. (j, k) *Ex vivo* stimulation of the splenocytes from immunized mice. (j) Representative flow cytometry plots and (k) percentage of OT-I CD8$^+$ T cells producing IFN-γ and IL-2 in the spleen following stimulation with the OVA (257−264) peptide for 5 h *in vitro* were shown. Mean ± s.e. is shown by the bars together with the symbols representing the individual data. Data are pooled from (g,i) two independent experiments or (k) one representative of two independent experiments. **; $p < 0.01$ and **; $p < 0.0001$.**

extracts compared to that of the positive control group injected with lipopolysaccharide (LPS) at 6 h after administration (Figure 4d). Time-dependent IL-6 production was evaluated at 2, 4, 6, 8, 18, and 36 h after administration. The IL-6 production that was induced by the empty-LNP$_{ssPalmE}$ peaked at 6 h and then diminished within 36 h (Figure 4e). The production of IL-6 was dependent on the route of administration (Figure S10): in the case of the intravenous injection of the empty-LNP$_{ssPalmE}$, the production of IL-6 was negligible from 2 to 36 h (Figure 4g). These results suggest that the strong activation of innate immunity induced by the vitamin E scaffolds was specific to the site of administration in the skin or the muscle.

Type I Interferon Signaling Is Involved in the LNP$_{ssPalmE}$-Induced CD8$^+$ T Cell Response. To gain insights into signaling pathways activated by the LNP$_{ssPalmE}$, we performed an RNA-seq analysis of the skin and draining lymph nodes 1 day after the administration of the empty-LNP$_{ssPalmE}$, the mOVA-LNP$_{ssPalmE}$, the empty-LNP$_{ssPalmM}$, or PBS. The results clearly showed that the gene expression profiles of the empty-LNP$_{ssPalmE}$ administered tissue and mOVA-LNP$_{ssPalmE}$ administered tissue were similar to each

https://doi.org/10.1021/acsnano.3c02251
ACS Nano 2023, 17, 18758−18774

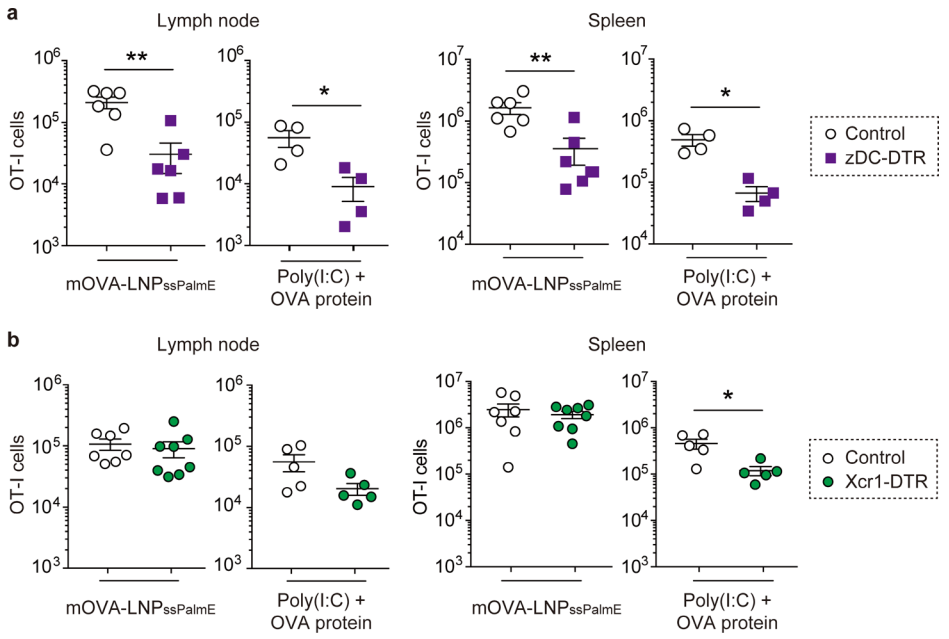

Figure 6. Essential role of cDCs but not cDC1s for the CD8$^+$ T cell response to the mRNA-LNP$_{ssPalmE}$. (a,b) Antigen-dependent expansion and their differentiation to effector cells of CD8$^+$ T cells. OT-I CD8$^+$ T cells were transferred into control (a, b), (a) zDC-DTR, or (b) Xcr1-DTR bone marrow chimeras that were subsequently immunized with poly(I:C) plus soluble OVA protein or mOVA-LNP$_{ssPalmE}$. Numbers of transferred OT-I CD8$^+$ T cells in the draining lymph nodes and spleen were assessed by flow cytometry 7 d after immunization. The mean ± s.e. is shown by the bars together with the symbols representing the individual data. Data are pooled from two independent experiments. *; $p < 0.05$ and **; $p < 0.01$.

other (Figure 5a−c). However, they were quite distinct from the profile for the empty-LNP$_{ssPalmM}$ administered tissue, which resembled the profile of the PBS-administered tissue (Figure 5a−c). These observations confirm that the ionizable lipids with vitamin E, rather than the encapsulated IVT-mRNA, have an important role in activating the responses at the injection site. A gene ontology analysis suggested that the type I interferon signaling pathways were activated in the empty-LNP$_{ssPalmE}$ administered tissue (Figure 5d,e). We, therefore, tested the effect of inhibiting type I interferon receptor signaling on the mOVA-LNP$_{ssPalmE}$ induced OT-I CD8$^+$ T cell response by using a blocking antibody against the interferon-α/β receptor α chain (anti-IFNAR-1 mAb). Although the number of OT-I CD8$^+$ T cells in the draining lymph nodes at 7 days after immunization remained unchanged by the treatment with anti-IFNAR-1 mAb, that in the spleen was significantly reduced (Figure 5f,g). The downregulation of CD62L$^+$ on OT-I CD8$^+$ T cells was suppressed by the anti-IFNAR-1 mAb treatment in both the lymph nodes and the spleen (Figure 5h,i). The capability of activated OT-I CD8$^+$ T cells to produce IL-2 and IFN-γ was also suppressed by the anti-IFNAR-1 mAb treatment (Figure 5j,k). These results suggest that the activation of type I interferon signaling pathways by the LNP$_{ssPalmE}$, probably by its vitamin E scaffold, contributes to the effector cell differentiation of antigen-specific CD8$^+$ T cells induced by the LNP$_{ssPalmE}$.

Conventional DCs Are Required for LNP$_{ssPalmE}$ RNA Vaccine-Induced CD8$^+$ T Cell Response. We also attempted to identify the cell types responsible for the antigen presentation to CD8$^+$ T cells after immunization with mRNA-LNP$_{ssPalmE}$. Since conventional dendritic cells (cDCs) were the candidates for cells responsible for the antigen presentation,[36] we transferred OT-I CD8$^+$ T cells into zDC-DTR bone marrow chimeric mice in which cDCs could be depleted upon treatment with a diphtheria toxin (DT). It was found that the OT-I CD8$^+$ T cell expansion at 7 days after immunization with mOVA-LNP$_{ssPalmE}$ or with the OVA protein plus poly(I:C) was much smaller in DT-treated zDC-DTR bone marrow chimeras than that in DT-treated control bone marrow chimeras (Figure 6a). These results suggest that cDCs are responsible for the antigen presentation to CD8$^+$ T cells after immunization with mRNA-LNP$_{ssPalmE}$. We then examined the requirement for cDC1s, which are a subset of cDCs that are capable of cross-presentation of exogenous antigens to MHC-I. For this purpose, we transferred OT-I CD8$^+$ T cells into Xcr1-DTR bone marrow chimeras in which cDC1s could be depleted upon a DT treatment.[37,38] In general, the antigen presentation of extracellular proteins on MHC-I requires cross-presentation by the cDC1s. As expected, the OT-I CD8$^+$ T cell expansion in response to OVA protein plus poly(I:C) was smaller in DT-treated Xcr1-DTR bone marrow chimeras than in DT-treated control bone marrow chimeras (Figure 6b). In contrast, intact OT-I CD8$^+$ T cell expansion in DT-treated Xcr1-DTR bone marrow chimeras that had been immunized with mOVA-LNP$_{ssPalmE}$ was observed (Figure 6b). This suggests that the antigen presentation by cDC1s is not essential for the CD8$^+$ T cell response to the mRNA-LNP$_{ssPalmE}$, and that cDC2s are considered to be involved in antigen presentation.

Migratory cDC2s Are the Main cDCs Subset Expressing mRNA-LNP$_{ssPalmE}$-Derived Antigen. The above results point to the possibility that cDC2s directly take up the mRNA-LNP$_{ssPalmE}$ and then express antigen encoded in the IVT-mRNA, since they are generally incapable of cross-presentation and their MHC-I molecules only present a self-antigen-derived peptide. To identify the cell types that express the antigen encoded in the IVT-mRNA encapsulated in the mRNA-LNP$_{ssPalmE}$ in draining lymph nodes, we prepared an mRNA-LNP$_{ssPalmE}$ containing Cre recombinase-coding mRNA (mCre-

https://doi.org/10.1021/acsnano.3c02251
ACS Nano 2023, 17, 18758−18774

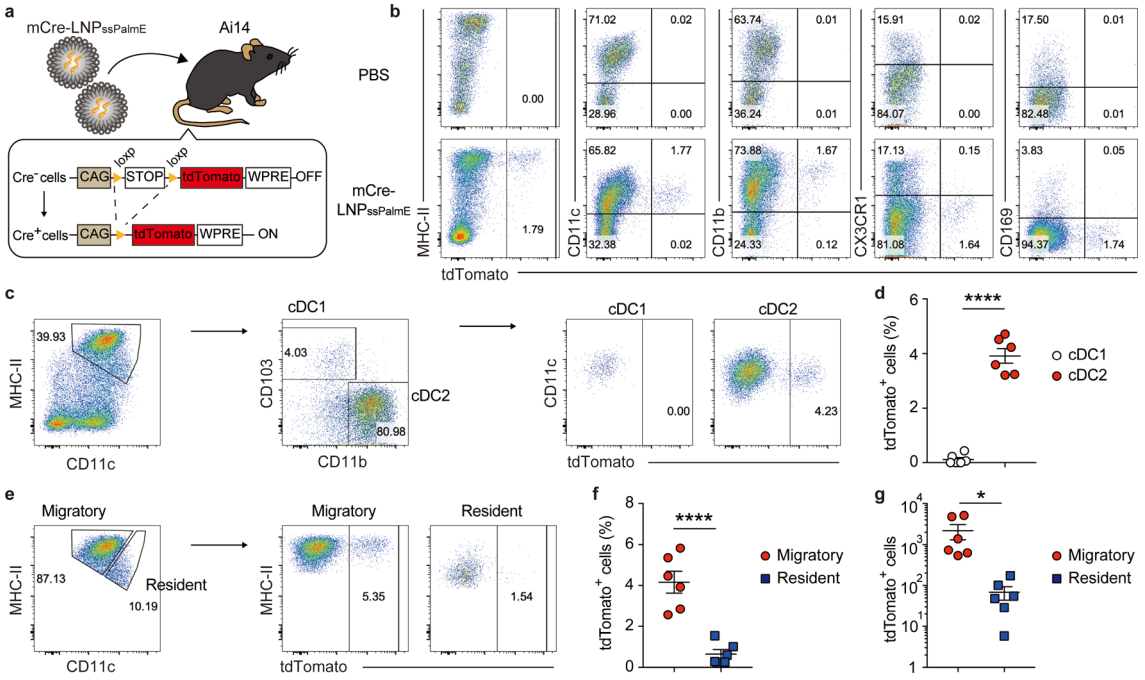

Figure 7. Identification of main cell type expressing the $LNP_{ssPalmE}$ RNA vaccine-derived antigen in the draining lymph node. (a) Schematic representation of the experimental design. (b–g) Flow cytometry of tdTomato$^+$ cells in the NK1.1$^-$ CD19$^-$ TCRβ^- TCR$\gamma\delta^-$ populations isolated from the lymph nodes of Ai14 mice 3 days after PBS or mCre-$LNP_{ssPalmE}$ injection. (b) Expression of tdTomato and cell surface makers. (c) Flow cytometry and (d) percentage of tdTomato$^+$ cells in CD103$^+$ cDC1 and CD11b$^+$ cDC2 population, (e) representative flow cytometry plot, (f) percentage, and (g) number of tdTomato$^+$ cells in MHC-II^{hi} migratory DC and MHC-II^{lo} resident DC population were shown. The mean ± s.e. is shown by the bars together with the symbols representing the individual data. (d, f, g) Data are pooled from two independent experiments. *; $p < 0.05$ and **; $p < 0.0001$.**

$LNP_{ssPalmE}$) and subcutaneously injected it into the foot pads of Ai14 mice in which Cre-expressing cells can be monitored by tdTomato fluorescence (Figure 7a).[39] Three days after the administration, flow cytometry detected tdTomato$^+$ cells, which had expressed the mRNA-LNPs-derived Cre protein, in popliteal lymph nodes of the Ai14 mice that had been injected with the mCre-$LNP_{ssPalmE}$ but not in PBS-injected mice (Figure 7b). The tdTomato$^+$ cells were largely positive for CD11c and CD11b, and were negative for CX3CR1, CD169, or CD103, suggesting that the majority of cells that expressed mRNA-LNPs-derived Cre protein in the draining lymph nodes were cDC2s (Figure 7b–d). We also found that the tdTomato$^+$ cells were enriched in the MHC-II^{hi} population compared to the MHC-II^{int} population, suggesting that they were migratory cDC2s derived from the skin (Figure 7e–g).[40] These collective results suggest that cDC2s in the skin take up subcutaneously injected mRNA-$LNP_{ssPalmE}$, express antigen encoded in the IVT-mRNA, and then migrate to the draining lymph nodes.

DCs Expressing Antigen Derived from mOVA-$LNP_{ssPalmE}$ Make Antigen-Dependent Contacts with CD8$^+$ T Cells. To directly confirm that the migratory cDC2s expressing antigen proteins are indeed involved in the priming of antigen-specific CD8$^+$ T cells in the lymph node, antigen-dependent contact between transfected cDC2s and CD8$^+$ T cells was examined by an imaging-based approach. We prepared $LNP_{ssPalmE}$ containing IVT-mRNA for the OVA/Cre fusion protein conjugated with the self-cleaving T2A peptide sequence in between ($mOVA_{T2A}Cre$-$LNP_{ssPalmE}$) (Figure 8a). This strategy was designed to ensure that every cell visualized by the Cre-dependent reporter also expressed OVA. $mOVA_{T2A}Cre$-$LNP_{ssPalmE}$ was injected into the foot pads of CD11c-YFP Ai14 mice which harbor both the DC-selective YFP reporter gene and the Cre-dependent tdTomato reporter gene. Two days later, Far Red dye-labeled OT-I CD8$^+$ T cells were intravenously transferred to the immunized CD11c-YFP Ai14 mice, and were allowed to enter the lymph nodes over a period of 2 h until an anti-CD62L mAb injection to inhibit further lymphocyte entry into the skin-draining lymph nodes.[37] The popliteal lymph nodes were harvested 13–14 h after the injection of the anti-CD62L mAb such that all of the OT-I CD8$^+$ T cells in the harvested lymph nodes had dwelled in the lymph nodes for 13–16 h and had sufficient time to interact with DCs (Figure 8a). We measured the number of OT-I CD8$^+$ T cells in contact with each CD11c-YFP$^+$ tdTomato$^+$ cell in the lymph node sections. The findings indicated that nearly 50% of the CD11c-YFP$^+$ tdTomato$^+$ cells had been in contact with at least one OT-I CD8$^+$ T cell and that at least 20% had been in contact with multiple OT-I CD8$^+$ T cells (Figure 8b,c). To evaluate the frequency of antigen-independent contact, we conducted a control analysis in parallel using mCre-$LNP_{ssPalmE}$ and the results showed that the frequency of CD11c-YFP$^+$ tdTomato$^+$ cells in contact with OT-I CD8$^+$ T cells was clearly smaller than that of $mOVA_{T2A}Cre$-$LNP_{ssPalmE}$ (Figure 8b,c). These results together with the flow cytometry results described above suggest that migratory cDC2s expressing antigen derived from mRNA-$LNP_{ssPalmE}$ present the antigen on MHC-I molecules to induce the CD8$^+$ T cell response.

DISCUSSION

In this study, we demonstrated that mRNA-LNPs prepared with ionizable lipids containing a vitamin E scaffold could be used as a material for an RNA vaccine against cancer and

https://doi.org/10.1021/acsnano.3c02251
ACS Nano 2023, 17, 18758–18774

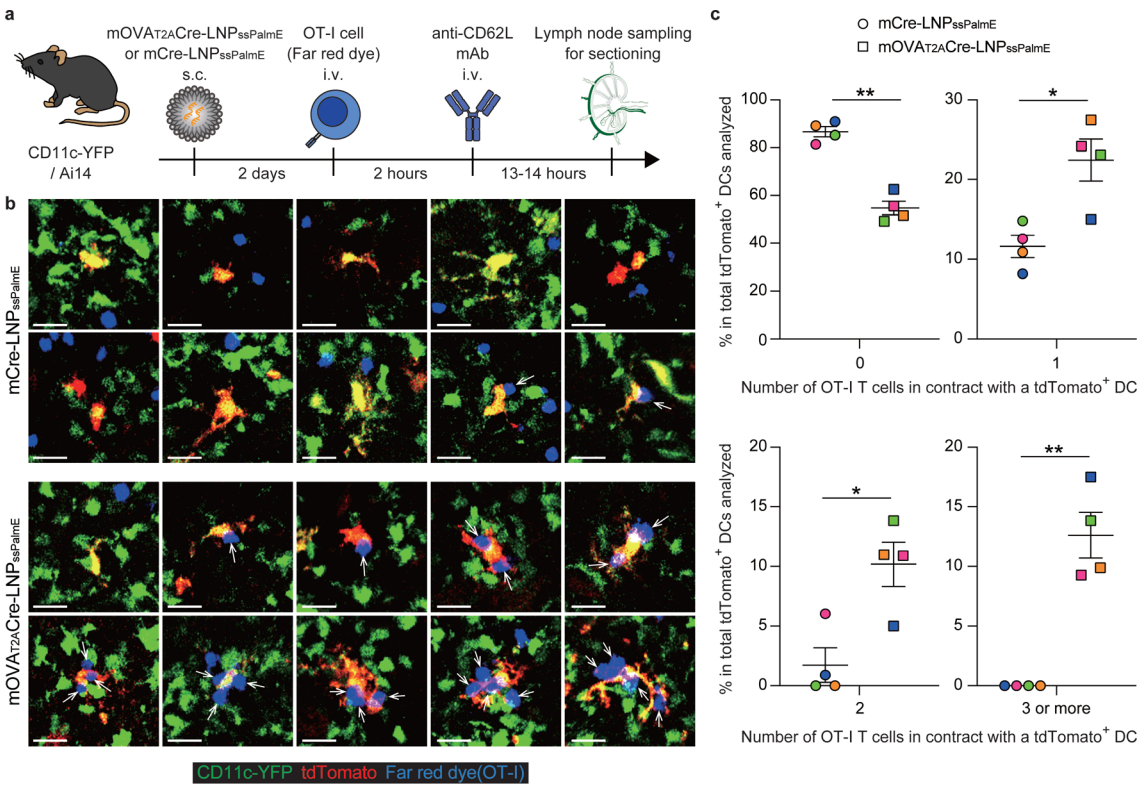

Figure 8. Antigen-dependent contacts of DCs expressing antigen derived from mRNA-LNP$_{ssPalmE}$ with CD8$^+$ T cells. (a) Schematic showing the time course for the vaccination of CD11c-YFP Ai14 mice into foot pads, adoptive transfer of Far Red dye-labeled OT-I CD8$^+$ T cells, administration of anti-CD62L antibody to inhibit further entry of lymphocytes into lymph nodes, and sampling of draining, popliteal lymph nodes. (b) Representative confocal microscopy images (12 μm projection depth) of nontransduced DCs (green), LNP$_{ssPalmE}$ RNA vaccine-transduced DCs (yellow-red), and OT-I CD8$^+$ T cells (blue) in draining lymph node sections. Arrows indicate OT-I CD8$^+$ T cells in contact with the transduced DCs. Scale bars indicate 20 μm. (c) Frequencies of transduced DCs in contact with the indicated numbers of OT-I CD8$^+$ T cells. The mean ± s.e. is shown by the bars together with the symbols representing the individual data. The data are from 4 independent experiments represented by 4 colors of the symbols. *; $p < 0.05$ and **; $p < 0.01$.

parasitic infections. Our results indicate that the enhanced adjuvant activity of the RNA delivery system for cellular immunity represents a potential strategy for treating these diseases. The optimized lipid composition of the mRNA-LNP$_{ssPalmE}$ that showed the highest CTL activity was ssPalmE-P4C2/DOPE/Cholesterol = 60/30/10 with an additional 3 mol % of DMG-PEG$_{2000}$. This high CTL activity cannot be simply explained from the point of view of *in vivo* mRNA transfection efficiency since the optimized LNP$_{ssPalmE}$ showed a lower luciferase activity than the control composition with a lower CTL activity (i.e., ssPalmE/DOPE/Cholesterol = 30/30/40, Figure S11). This observation confirms the notion that the efficiency of gene expression is not only an important property of mRNA-LNPs for vaccine use: immune activation is a prerequisite for inducing adaptive immunity. The higher adjuvant activity of the optimized LNP$_{ssPalmE}$, presumably due to the larger ssPalmE content, might compensate for the decreased transfection activity and contribute to eliciting an overall higher CTL activity (Figure 4a,c).

The activation of innate immunity is generally triggered by the stimulation of pattern recognition receptors (PRRs).[7,41−44] Therefore, one possible component of the mRNA-LNPs for the activation of innate immunity has been considered to be the IVT-mRNA molecule, since the presence of intracellular/extracellular nonself RNA molecules is recognized as a sign of invasion by pathogenic microorganisms.[45] Actually, an IVT-mRNA has a key role in the activation of antigen-specific immunity via the Toll-like receptor 7 (TLR7) in the case of a lipoplex-type RNA vaccine.[20,46] In contrast, in our experiments, the stimulation of the innate immunity (Figure 5a−c) and the activation of the T cells (Figure 4a,c) were mainly induced by the LNPs. Co-stimulatory molecules such as CD86 and CD40 on the DCs in draining lymph nodes were also upregulated by the subcutaneous injection of the empty-LNP$_{ssPalmE}$ (Figure S12).[47] Therefore, it is plausible that not the IVT-mRNA but rather the LNP$_{ssPalmE}$ is the main substance causing the immune stimulation. Further analysis using other ssPalm derivatives (ssPalmM-P4C2 and ssPalmO-P4C2) revealed that the LNPs-derived innate immune response was highly dependent on its hydrophobic scaffolds (Figure 4d,f). Only LNP$_{ssPalmE}$ caused a significant production of IL-6 when injected into the skin.

An important observation was that the production of inflammatory cytokines was dependent on the route of administration. While the subcutaneous injection of the LNP$_{ssPalmE}$ caused significant IL-6 production, the intravenous injection of the same particle resulted in only the marginal production of IL-6 (Figure 4g, Figure S3). It was also reported that stronger IL-6 production was induced after subcutaneous injection compared to intravenous injection in the case of other LNPs.[48,49] This injection site-limited inflammation of the mRNA-LNPs is quite important in terms of safety. Even if the LNPs leaked from the injection site to the blood circulation, they might not induce further systemic inflammation.

https://doi.org/10.1021/acsnano.3c02251
ACS Nano 2023, 17, 18758−18774

It was previously reported that IL-6 plays a key role in the differentiation of naïve CD4$^+$ T cells to follicular helper T cells (Tfh),[50] an important population of cells for humoral immunity. Inhibition of the IL-6 pathway resulted in fewer Tfh cells and germinal center B cells (GC B cells) in the case of other LNPs.[22] Considering the strong IL-6 induction ability of LNP$_{ssPalmE}$, mRNA-LNP$_{ssPalmE}$ might also have favorable characteristics as an RNA vaccine against extracellular infectious microorganisms. In addition to IL-6 production, KC, MCP1, and IP-10 were increased by the injection of LNP$_{ssPalmE}$ (Figure S9). This observation is consistent with the previous literatures which showed infiltration of neutrophils/monocytes to the injection site of LNPs.[19,51]

Another important characteristic of LNP$_{ssPalmE}$ was the activation of type I interferon responses derived from the vitamin E scaffolds. Type I interferons play important roles in survival and effector differentiation during the clonal expansion of CD8$^+$ T cells by acting on DCs and CD8$^+$ T cells.[52−56] Consistently, our anti-IFNAR-1 antibody blockade experiments suggested that the LNP$_{ssPalmE}$-induced type I interferon responses are particularly important for the effector differentiation of antigen-engaged CD8$^+$ T cells after immunization with the mRNA-LNP$_{ssPalmE}$. Since the production of IFN-β by the LNP$_{ssPalmE}$ was not observed in serum at 6 h after the s.c. injection, the production of this interferon was probably limited to the site of injection. In the case of an RNA vaccine against SARS-CoV-2 produced by Pfizer-BioNTech, a type I interferon signal was induced in mice and was critical for achieving cellular immunity. In this report, they claimed that the cytosolic sensor MDA5, which recognizes dsRNA, had a key role in type I interferon signaling and cellular immunity.[21] In contrast, in the case of LNP$_{ssPalmE}$, type I interferon signaling was induced even in the absence of encapsulated mRNA (Figure 5d), presumably by the chemical structure of the lipids in the preparation. Therefore, the incorporation of vitamin E into the structure of the ionizable lipid represents a potentially promising strategy for activating type I interferon signals regardless of the properties of cargo IVT-mRNA. The cell types that produce type I interferons in the skin and draining lymph nodes in response to LNP$_{ssPalmE}$ are currently unclear although fibroblastic cells, macrophages/monocytes, and DCs are likely candidates.[57]

Vitamin E has been employed as a component of the approved adjuvant AS03.[58,59] In experiments with mice, proinflammatory cytokines and chemokines such as IL-6, IL-1β, and CCL2 were secreted after intramuscular injection. Based on *in vitro* measurements, monocytes and macrophages appear to be involved in the secretion of these molecules. On the other hand, the production of type I interferon was not observed at the injection sites and draining lymph nodes after the administration of AS03.[59] Therefore, the incorporation of the α-tocopherol moiety into the structure of the ionizable lipid might confer an additional immune-stimulative function to the LNPs. The incorporation of ssPalmE-P4C2 into the lipid composition of LNP$_{ssPalmM}$ resulted in an increased production of CXCL1 (Figure S13). The production of IL-6 also tended to increase when ssPalmE-P4C2 was incorporated. On the other hand, the incorporation of α-tocopherol or α-tocopherol succinate to the LNP$_{ssPalmM}$ resulted in no increase in such cytokines/chemokines. This observation indicates that the ssPalmE-P4C2 which contains an ionizable lipid with vitamin E in its scaffold appears to be important for this adjuvant activity. It is noteworthy that extracellular dsDNA was detected in the empty-LNP$_{ssPalmE}$ group from the lavage of skin samples at 6 h after the administration (Figure S14). dsDNA in the extracellular region could be regarded as damage associated molecular patterns (DAMPs) and that cause an innate immune response.[60] HP-β-cyclodextrin, which was originally utilized to improve the solubility of hydrophobic compounds, elicited an adjuvant effect by inducing the release of DAMPs after intradermal injection. After the injection of HP-β-cyclodextrin, type I interferon was induced in the draining lymph nodes. Our data suggest that LNP$_{ssPalmE}$ might induce innate immunity by a similar DAMPs-dependent mechanism.[61]

The activation of the antigen-specific CD8$^+$ T cells requires antigen presentation on MHC-I by APCs. When the RNA vaccine is topically administered, a large part of antigen protein is expressed by nonimmune cells at the administration site.[48] Therefore, as in the case of a conventional protein vaccine, the contribution of cross-presentation by APCs might be assumed: expressed extracellular antigens are taken up by the APCs, and the antigen is then degraded to a peptide via the vacuolar pathway and/or the endosome-to-cytosol pathway for antigen presentation by MHC-I.[62] Meanwhile, in the case of an RNA vaccine, it is also plausible that the LNPs *per se* are taken up to the APCs, and thereafter, the antigen proteins are expressed in the APCs.[9,15,63] In this case, the proteasome degrades the intracellular antigen into peptides, and the resulting peptides are then transported to the endoplasmic reticulum (ER) for the antigen presentation on MHC-I directly or after editing by ER aminopeptidases associated with antigen processing (ERAAP).[64] However, the issues of which mechanism mainly contributes to the induction of cellular immunity by subcutaneous injection of mRNA-LNPs and, moreover, which subset of cells function as APCs remain to be elucidated.

Our results indicate that cDCs are essential for the response of CD8$^+$ T cells to mRNA-LNP$_{ssPalmE}$ and that cDC1, a subset of cDCs, was not required. Therefore, cross-presentation is not the only and most likely not the major pathway of antigen-presentation by cDCs to CD8$^+$ T cells in response to mRNA-LNP$_{ssPalmE}$. Another possible pathway is that cDCs are directly transfected by the mRNA-LNP$_{ssPalmE}$ and the vaccine-derived antigens are presented on the MHC-I complex as their autoantigens since it was confirmed that the mRNA-LNP$_{ssPalmE}$ could be taken up by bone marrow-derived DCs and induce gene expression (Figure S15). This hypothesis was strongly supported by the observation that DCs expressing the vaccine-derived antigens made antigen-dependent contacts with CD8$^+$ T cells (Figure 8). A similar antigen-presentation pathway to CD8$^+$ T cells was reported for vaccinia virus-infected cDCs.[65]

An important finding is that draining lymph node cells that are transfected by mRNA-LNP$_{ssPalmE}$ were mainly migratory cDC2s. This suggests that mRNA-LNP$_{ssPalmE}$ transfects cDC2s in the skin but does not efficiently reach the lymph node parenchyma to transfect lymph node-resident cDCs. On the other hand, it was reported that Langerhans cells and cDC1s have a key role in inducing humoral immunity via the intradermal injection of other LNPs.[51] The reason for why migratory cDC1s transfected by the mRNA-LNP$_{ssPalmE}$ were few in number in the draining lymph is currently unclear. One possibility is that migratory cDC1s transfected by mRNA-LNP$_{ssPalmE}$ might become prone to die. Another possibility is that cDC1s are ineffectively transfected by the mRNA-LNP$_{ssPalmE}$. The latter may be more likely because acidification in endosomes of cDC1s is known to be restricted in terms of achieving efficient cross-presentation[62,66] and may not be

https://doi.org/10.1021/acsnano.3c02251
ACS Nano 2023, 17, 18758−18774

sufficient for the endosomal escape of the mRNA-LNP$_{ssPalmE}$. Future studies will need to address these possibilities if we are to fully understand the mechanism responsible for how mRNA-LNP$_{ssPalmE}$ induces efficient CTL responses.

CONCLUSION

In this study, we demonstrated that a vitamin E scaffold in ionizable lipids acts as an adjuvant that stimulates type I interferon signaling, at least in part due to their ability to induce DAMPs. This stimulation of innate immunity, as well as the production of antigen proteins in the cytoplasm of cDC2s, is an important property of the mRNA-LNP$_{ssPalmE}$ as an RNA vaccine. The addition of biological functions to ionizable lipids by modifying their chemical structure is a promising strategy for expanding the area of therapeutic application of mRNA-LNPs.

METHODS

Mice. Female C57BL/6J and BALB/c mice, aged 6−10 weeks, were purchased from Nippon SLC, Inc. (Shizuoka, Japan). The breeding and experiments were conducted under the guidelines for handling experimental animals, approved by the Animal Care Committee of Chiba University and Tohoku University.

The experimental design of infection experiments was approved by the Committee on the Ethics of Animal Experiments at the Obihiro University of Agriculture and Veterinary Medicine (permission numbers 20-181).

OT-I (003831), Ai14 (007908), CD11c-YFP (008829), zDC-DTR (019506), and CD45.1 congenic (002014) mice were obtained from Jackson Laboratory. The Xcr1-DTR mice have been described previously[38] and are available from the RIKEN BioResource Research Center (RBRC09485). C57BL/6J mice were obtained from CLEA Japan. All animal studies using these mice were performed in accordance with the guidelines of the Animal Experiment Committee of the RIKEN Yokohama Institute.

Cell Culture. E.G7-OVA cells, the murine lymphoma cell line EL4 expressing OVA, were purchased from the American Type Culture Collection (Manassas, VA, USA). E.G7-OVA cells were cultured in RPMI-1640 medium supplemented with 10% (v/v) FCS, 50 μM 2-mercaptoethanol, 10 mM HEPES, 1 mM sodium pyruvate, 400 μg/mL G418 Sulfate (FUJIFILM Wako Pure Chemicals, Osaka, Japan), and 100 U/mL penicillin−streptomycin. The cells were collected and cultured in a separate dish with fresh medium every 2 days (cell passage). The cells were used in experiments after the third cell passage.

***In Vitro* mRNA Transcription.** The pcDNA3.1 vector was used as a coding template for ovalbumin (OVA), Luciferase (Luc), *Toxoplasma gondii* profilin (TgPF), Cre recombinase (Cre), and Ovalbumin-T2A-Cre recombinase (OVA$_{T2A}$Cre). The pT7 vector was used as a coding template for *T. gondii* profilin (TgPF). The pcDNA3.1-OVA or pcDNA3.1-OVA$_{T2A}$Cre were linearized with the restriction enzyme XhoI (New England Biolabs, Massachusetts, US) and the pcDNA3.1-Luc or pcDNA3.1-Cre were linearized with the restriction enzyme BspEI (New England Biolabs, Massachusetts, US), respectively. After phenol-chloroform extraction and ethanol precipitation, the linearized pDNA was transcribed into mRNA by an mMESSAGE mMACHINE T7 ULTRA Transcription kit (Life Technologies, Carlsbad, CA, USA) following the manufacturer's instructions. The transcribed mRNA was stored in THE RNA Storage Solution (Invitrogen, Waltham, MA, US) at −80 °C. The concentration of linearized pDNA and transcribed mRNA were measured by NanoDrop One (Thermo Fisher Scientific, Waltham, MA, US). mOVA, mLuc, mCre, and mOVA$_{T2A}$Cre were unmodified. mTgPF was modified by m1ψ.

LNP Synthesis. COATSOME SS-EC (ssPalmE-P4C2), ssPalmM-P4C2, ssPalmO-P4C2, and 1,2-dimyristoyl-rac-glycero-3-methoxypolyethylene glycol) 2000 (SUNBRIGHT GM-020) were provided by the NOF CORPORATION (Tokyo, Japan). The 1,2-dioleoyl-*sn*-glycero-2-phosphoethanolamine (DOPE) was purchased from Avanti Polar Lipids, Inc. (Alabaster, AL, USA). Cholesterol was purchased from Sigma-Aldrich (St. Louis, MO, US).

When the LNPs were prepared by vortex mixing, lipid mixtures dissolved in 99.5% EtOH were prepared in 5 mL tubes. Arbitrary ratio of ssPalmE-P4C2, DOPE, and Cholesterol was included in the tube to become 131.5 nmol Lipid in total, and 3 mol % of DMG-PEG$_{2000}$ was added to the tube. These lipid mixtures were adjusted their volume to 30 μL. Three μg of mRNA was dissolved in 45 μL of 20 mM Malic acid and 100 mM NaCl buffer (pH 3.0). mRNA solution was added to the tube containing the lipid mixture in vortex condition and then 925 μL of 20 mM MES buffer (pH 5.5) was added to that. Vortex mixing was kept for 10 s after the MES buffer was added to the tube.

When the LNPs were prepared by microfluidic device, the lipid mixture and mRNA solution in their respective syringes were placed into the iLiNP device.[32] In the case of the optimized condition, the flow rate was set at 300 μL/min for the lipid mixture and 450 μL/min for mRNA solution, the lipid composition was ssPalmE-P4C2/DOPE/Cholesterol; DMG-PEG 2000 = 60/30/10; 3 mol % of total lipid, and the total lipid concentration was 394.5 nmol, encapsulating 3 μg of mRNA (lipid/mRNA: 131.5 nmol/μg). The lipid mixtures and mRNAs were dissolved in 99.5% Ethanol and 20 mM Malic acid buffer pH 3.0: 30 mM NaCl, respectively. After that the same volume of 20 mM MES buffer (pH 5.5) was added in vortex condition.

The buffer of LNP was changed to D-PBS (−) by ultrafiltration using AmiconUltra-4−100 K (Merck, Darmstadt, Germany) and repeated centrifugation at 25 °C, 1000 G, 5 min. Particle size, zeta potential, and PdI of the LNP were measured by a Zetasizer Nano ZS (Malvern Instruments Ltd., Malvern, UK). The encapsulation and recovery rates were evaluated by the RiboGreen Assay.

Cryo-EM Imaging. Cryo-EM images were collected using a cryo-EM, Talos Arctica (FEI, Netherlands) with an accelerating voltage of 200 kV. The cryo-EM is equipped with a Falcon III direct electron detector (FEI, Netherlands). The cryogrids for cryo-EM imaging were prepared using a Vitrobot IV (FEI, Netherlands). The grids (Quantifoil Cu R1.2/1.3 300 mesh) were glow discharged for 45 s to hydrophilize the surface of the grid before use. Three μL of the LNP suspension (20 mM total lipids in Nuclease-free water) was deposited on a grid at 4 °C and 100% humidity. The excess volume of the suspension was removed by the blotting of filter papers. Then, the grid was rapidly vitrified with liquid ethane. The prepared grids were used for cryo-EM image collection.

RiboGreen Assay. Six standard samples with 2000, 1000, 500, 250, 125, and 0 ng/mL concentrations of mRNA solutions in D-PBS (−) were made. The LNP solutions were diluted in D-PBS (−) to a concentration equivalent to 1000 ng/mL of mRNA. Solutions containing Quant-iT RiboGreen RNA reagent (Invitrogen, Waltham, MA, US) and 10% (v/v) TritonX-100 with 1:8 ratios were prepared in D-PBS (−): Triton [-] (no TritonX-100, only RiboGreen) and Triton [+] (contained both RiboGreen and TritonX-100). As much as 50 μL of diluted LNP solutions was each applied two times on the 96-well black microplate (Corning, Cambridge, MA, US). A 50 μL aliquot of Triton [-] was added to one well, and the other received 50 μL of Triton [+]. The fluorescence intensities were analyzed by plate reader Infinite M200 PRO (TECAN, Männedorf, Switzerland) set with emission and excitation waves of 484 and 535 nm, respectively.

Cell Isolation, Adoptive Transfer, and Immunization. Spleen and peripheral lymph node cells were harvested from OT-I mice by mashing through 70 μm nylon cell strainers (BD Biosciences, San Jose, CA, US). The single cell suspension containing 1 × 10^5 TCRVα2$^+$ CD8$^+$ T cells of OT-I mice (CD45.1) was injected iv to C57BL/6J mice (CD45.2). The mice were immediately immunized s.c. with 10 μg of OVA (Sigma-Aldrich, St. Louis, MO, US), 25 μg of the OVA protein plus 12.5 μg of poly(I:C) (GE Healthcare, Chicago, IL, US), or mOVA-LNP$_{ssPalmE}$ (0.2 μg, 1.5 μg, or 3.0 μg of mRNA) in 100−200 μL of PBS into the base of the tail.

For blocking experiments of type-I interferon receptor signaling, 0.5 mg of an anti-IFNAR-1 neutralizing antibody (MAR1−5A3; Bio X Cell, Lebanon, NH, US) or isotype control antibody (mouse IgG1;

https://doi.org/10.1021/acsnano.3c02251
ACS Nano 2023, 17, 18758−18774

Bio X Cell, Lebanon, NH, US) was injected i.p. in 200 μL of PBS 1 day prior to immunization.

For DC-depletion experiments, C57BL/6J wild-type mice (CD45.2) were lethally irradiated (9.5 Gray) and injected iv with 2 × 10^6 total bone marrow cells isolated from zDC-DTR mice (CD45.1) or Xcr1-DTR mice (CD45.2). The mice bone marrow cells that were reconstituted for a minimum of 8 weeks after irradiation were injected i.p. with diphtheria toxin (Sigma-Aldrich, St. Louis, MO, US) 1 day prior to immunization (500 ng in 100 μL PBS) and 2 and 5 days after immunization (300 ng in 100 μL PBS). For zDC-DTR bone marrow chimera experiments, tdTomato$^+$ OT-I CD8$^+$ T cells were used.

For imaging experiments, single-cell suspensions of spleen and lymph node cells were prepared, and non-CD8$^+$ T cells were labeled with biotinylated linage cocktail antibodies obtained from BioLegend (San Diego, CA, US): anti-B220 (RA3−6B2), anti-CD4 (RM4−5), anti-CD11b (M1/70), anti-CD11c (HL3), anti-Gr-1 (RB6−8C5), and anti-TER119 (TER119), followed by Streptavidin MicroBeads (Miltenyi Biotec, Bergisch Gladbach, Germany). Unlabeled CD8$^+$ T cells were purified with an AutoMACS separator (Miltenyi Biotec, Bergisch Gladbach, Germany). The purified OT-I CD8$^+$ T cells were labeled with 1 μM CellTrace Far Red (Life Technologies, Carlsbad, CA, US) and 5 × 10^5 OT-I CD8$^+$ T cells were transferred i.v. into CD11c-YFP-Ai14 mice. The mice were then immunized s.c. in the footpad on both hind legs with mCre-LNP$_{ssPalmE}$ (0.75 μg of mRNA) or mOVA$_{T2A}$Cre-LNP$_{ssPalmE}$ (1.5 μg of mRNA) per site. Mice were treated i.v. with 100 μg of anti-CD62L antibody (MEL-14; BioLegend, San Diego, CA, US) at 2 h postimmunization to block entry of circulating lymphocytes into lymph nodes.

CTL Assay. *In vivo* CTL assay was performed as described previously.[28,67] Briefly, the mOVA-LNP$_{ssPalmE}$ was injected (s.c.) into C57BL/6J mice that had been anesthetized. After 7 days, splenocytes were prepared from naïve C57BL/6 mice and incubated with the OVA H-2K^b cytotoxic T-lymphocyte epitope peptide (SIINFEKL, OVA$_{257-264}$) at 37 °C for 1 h. The suspension of OVA$_{257-264}$ peptide-treated splenocytes was then labeled with 5.0 μM CFSE in D-PBS (−) at 37 °C for 10 min (CFSE^{high}, target cells). Another suspension of naïve splenocytes, untreated with the OVA$_{257-264}$ peptide, was labeled with 0.5 μM CFSE in D-PBS (−) at 37 °C for 10 min (CFSE^{low}, control cells). Each cell suspension was washed repeatedly with fresh medium and D-PBS (−), then resuspended in 5.0 × 10^7 cells/mL cells concentration in D-PBS (−). The cells were administered (i.v.) to the immunized mice with an equal volume (ratio 1:1) of CFSE^{high} and CFSE^{low}-labeled cells. After 20 h, splenocytes were collected from the immunized mice and single-cell suspensions were prepared. The number of the CFSE-labeled cells (CFSE^{high} and CFSE^{low}) was quantified by a NovoCyte Flow Cytometer (Agilent, Santa Clara, CA, USA). The degree of cell lysis was calculated as a ratio of the number of CFSE^{high} against CFSE^{low}-labeled cells.

Antitumor Effect against E.G7-OVA. E.G7-OVA cells (8.0 × 10^5 cells/40 μL) in D-PBS (−) were inoculated (s.c.) on the left flank of mice that had been anesthetized. After the tumor grew to ≥100 mm^3 (approximately after 7−9 days), the mice were immunized (s.c.) with LNP encapsulating 0.2 μg mOVA. Tumor size was measured at 3 days intervals with the calculation formula: [long axis] × [short axis]^2 × 0.52.

***T. gondii* Infection.** Mice were immunized with mTgPF-LNP$_{ssPalmE}$ (1.0 or 5.0 μg mRNA) or mLuc-LNP$_{ssPalmE}$ (5.0 μg mRNA) subcutaneously. Booster immunizations were performed 14 and 28 days after the first immunization. At 9 days after the third immunization, the mice of all groups were challenged intraperitoneally with 5 × 10^3 Pru HX-KU strain, *Toxoplasma gondii*. For end points, euthanasia by central destruction is performed before the animal becomes unconscious or unresponsive to external stimuli, when it loses more than 20% of its body weight, or when it has severe difficulty walking. The survival rates, Clinical scores, and Body weight of the mice were measured for 30 days. Survival curves were generated according to the Kaplan−Meier method, and statistical comparisons were made using the log-rank method using the GraphPad Prism version 5 (GraphPad Software, San Diego, CA). *P* values <0.05 were considered statistically significant.

ELISA. Mice were injected with the empty-LNP$_{ssPalmE}$, empty-LNP$_{ssPalmM}$, or LPS. Their blood was collected at the determined time after the injection and their serum were stored at −80 °C. Cytokine concentration in the serum was measured by ELISA kit (R&D systems, Minneapolis, US) according to the manufacturer's instructions. For the measurement of cytokines in the skin, 1.5 cm square skin tissues were collected at the injection site and homogenized with cell lysis buffer (ThermoFisher scientific, Massachusetts, US) by a micro smasher (TOMY SEIKO CO, Ltd., Tokyo, Japan). The protein concentration of the suspension was adjusted to 5 mg/mL protein by BCA protein assay (Takara Bio, Siga, Japan) and the cytokine concentration was measured by ELISA kit (RayBiotech Life, Inc., GA, USA).

Flow Cytometry. Single-cell suspensions were stained with the following fluorescent dye-labeled antibodies: CD8α (53−6.7), CD11b (M1/70), CD19 (6D5), CD62L (MEL-14), I-A/I-E (M5/114.15.2), IFN-γ (XMG1.2), IL-2 (JES6−5H4), NK1.1 (PK136), TCR$\gamma\delta$ (GL3), and TCRβ (H57−597) were obtained from Biolegends; CD11c (N418), CD44 (IM7), CD45.1 (A20), CD169 (SER-4), and CX3CR1 (SA011F11) were obtained from eBioscience: CD103 (M290) and TCRVα2 (B20.1) were obtained from BD Biosciences. Dead cells were stained with 7-AAD (Sigma-Aldrich) or Fixable Viability Dyes (eBioscience). For DC single-cell suspension, LNs were minced and treated with a 1 mg/mL solution of Collagenase Type 4 (Worthington Biochemical) and 100 μg/mL DNase I (Roche) for 30 min at 37 °C. For intracellular cytokine staining, splenocytes were stimulated with the OVA (257−264) peptide (5 or 500 pg/mL; ANASPEC) in the presence of GolgiStop (BD Biosciences) in PRMI 1640 supplemented with 10% FBS for 5 h. Surface-stained cells were fixed and permeabilized with a Cytofix/Cytoperm kit according to the manufacturer's instructions (BD Biosciences). The cells were analyzed on a FACSCanto II (Becton Dickinson), and data were analyzed using FlowJo software (Tree Star).

RNA Sequencing and Bioinformatics Analysis. Mice were immunized with empty-LNP$_{ssPalmM}$, empty-LNP$_{ssPalmE}$, or mOVA-LNP$_{ssPalmE}$ (1.2 μg of mRNA) into bilateral footpads and the top of the foot in 20 μL per site. Total RNA was extracted from the foot skin or the draining popliteal lymph nodes 1 day after immunization using TRIzol reagent (Life Technologies, Carlsbad, CA, US). The DNA library was constructed with a NEBNext Ultra II RNA Library Prep Kit for Illumina (New England Biolabs) according to the manufacturer's instructions. The DNA library was subjected to sequencing on a NextSeq 2000 sequencer (Illumina) in a 100-bp single-end read mode. The raw fastq data were quantified and mapped to the *Mus musculus* reference transcriptome GRCm39 (M30) using Salmon (v1.9.0). The transcript abundance counts were condensed to the gene level using the R package tximport (v1.20.0).[68] Data transformation, visualization, differential gene expression analysis, and pathway analysis were conducted through the iDEP (v0.96) web interface[69] that contains t-SNE,[70] DESeq2,[71] and GAGE[72] packages. To identify differentially expressed genes (DEGs), an absolute 2.5-fold-change difference between any two samples and false discovery rate (FDR) ≤ 0.1 were used. The top 2,000 genes were used for the k-means clustering analysis.

Confocal Microscopy and Image Analysis. The lymph nodes were fixed in 4% paraformaldehyde in PBS, placed in a Tissue-Tek OCT compound (Sakura), and frozen in dry ice. Cryostat sections (20 μm in thickness) were affixed to MAS-GP-coated slides (Matsunami Glass). YFP$^+$ cells, tdTomato$^+$ cells, and Far Red dye-labeled cells were detected by their fluorescence without staining. Images were acquired on a STELLARIS 5 upright microscope (Leica Microsystems).

Statistical Analysis. One-way ANOVA with Bonferroni's post-test was used for comparisons of more than two means (Figures 1d, 1f, 1g, 3b, 3d, 4a, 4c, 4d, and 4f). Unpaired two-tailed Student's *t*-test (Figures 3f, 3h, 3j, 4g, 5g, 5i, 5k, 6a, 6b, 7d, 7f, and 7g) or paired Student's *t*-test (Figure 8c) was used for comparisons of two means.

https://doi.org/10.1021/acsnano.3c02251
ACS Nano 2023, 17, 18758−18774

Log-rank tests (Figure 2b) were used for comparisons of the survival rate using the Kaplan−Meier method.

ASSOCIATED CONTENT

Supporting Information

The Supporting Information is available free of charge at https://pubs.acs.org/doi/10.1021/acsnano.3c02251.

List of information on suppliers of the reagents, supplementary figures (Figure S1−S15), and sequences of IVT-mRNA (PDF)

AUTHOR INFORMATION

Corresponding Authors

Takaharu Okada − *Laboratory for Tissue Dynamics, RIKEN Center for Integrative Medical Sciences, Yokohama City, Kanagawa 230-0045, Japan; Graduate School of Medical Life Science, Yokohama City University, Yokohama City, Kanagawa 230-0045, Japan*; Phone: +8145-503-7026; Email: takaharu.okada@riken.jp

Hidetaka Akita − *Laboratory of DDS Design and Drug Disposition, Graduate School of Pharmaceutical Sciences, Tohoku University, Sendai City, Miyagi 980-8578, Japan; Center for Advanced Modalities and DDS, Osaka University, Suita, Osaka 565-0871, Japan;* orcid.org/0000-0001-6262-2436; Phone: +8122-795-6831; Email: hidetaka.akita.a4@tohoku.ac.jp

Authors

Ryotaro Oyama − *Laboratory of DDS Design and Drug Disposition, Graduate School of Pharmaceutical Sciences, Chiba University, Chiba City, Chiba 260-0856, Japan*

Harumichi Ishigame − *Laboratory for Tissue Dynamics, RIKEN Center for Integrative Medical Sciences, Yokohama City, Kanagawa 230-0045, Japan*

Hiroki Tanaka − *Laboratory of DDS Design and Drug Disposition, Graduate School of Pharmaceutical Sciences, Tohoku University, Sendai City, Miyagi 980-8578, Japan*

Naho Tateshita − *Laboratory of DDS Design and Drug Disposition, Graduate School of Pharmaceutical Sciences, Chiba University, Chiba City, Chiba 260-0856, Japan*

Moeko Itazawa − *Laboratory for Tissue Dynamics, RIKEN Center for Integrative Medical Sciences, Yokohama City, Kanagawa 230-0045, Japan*

Ryosuke Imai − *Laboratory for Tissue Dynamics, RIKEN Center for Integrative Medical Sciences, Yokohama City, Kanagawa 230-0045, Japan; Division of Physiological Chemistry and Metabolism, Graduate School of Pharmaceutical Sciences, Keio University, Tokyo 105-8512, Japan*

Naomasa Nishiumi − *Laboratory of DDS Design and Drug Disposition, Graduate School of Pharmaceutical Sciences, Tohoku University, Sendai City, Miyagi 980-8578, Japan*

Jun-ichi Kishikawa − *Laboratory for Cryo-EM Structural Biology, Institute for Protein Research, Osaka University, Suita, Osaka 565-0871, Japan*

Takayuki Kato − *Laboratory for Cryo-EM Structural Biology, Institute for Protein Research, Osaka University, Suita, Osaka 565-0871, Japan*

Jessica Anindita − *Laboratory of DDS Design and Drug Disposition, Graduate School of Pharmaceutical Sciences, Chiba University, Chiba City, Chiba 260-0856, Japan*

Yoshifumi Nishikawa − *National Research Center for Protozoan Diseases, Obihiro University of Agriculture and Veterinary Medicine, Obihiro City, Hokkaido 080-8555, Japan*

Masatoshi Maeki − *Division of Applied Chemistry, Faculty of Engineering, Hokkaido University, Sapporo City, Hokkaido 060-8628, Japan;* orcid.org/0000-0001-7500-4231

Manabu Tokeshi − *Division of Applied Chemistry, Faculty of Engineering, Hokkaido University, Sapporo City, Hokkaido 060-8628, Japan;* orcid.org/0000-0002-4412-2144

Kota Tange − *DDS Research Laboratory, NOF CORPORATION, Kawasaki City, Kanagawa 210-0865, Japan*

Yuta Nakai − *DDS Research Laboratory, NOF CORPORATION, Kawasaki City, Kanagawa 210-0865, Japan*

Yu Sakurai − *Laboratory of DDS Design and Drug Disposition, Graduate School of Pharmaceutical Sciences, Tohoku University, Sendai City, Miyagi 980-8578, Japan*

Complete contact information is available at: https://pubs.acs.org/10.1021/acsnano.3c02251

Author Contributions

▶R.O., H.I., and H.T. contributed equally. All authors contributed to the writing of this manuscript was written through contributions of all authors. All authors have given approval to the final version of the manuscript.

Funding

H.A., T.O., M.M., and M.T. were supported by a JST CREST grant [JPMJCR17H1]. H.A. is also supported by AMED (JP223fa627002, 21am0401030h0001, 22am0401030h0002 and 23am0401030h0003), and partially by the JSPS KAKENHI [21K18320], The Asahi Glass Foundation and The Canon Foundation. T.O. is also supported by JST [Moonshot R&D] [Grant Number JPMJMS2025]. H.T. was supported by the JSPS KAKENHI [17H06558, 18K18377, 21K18035], and Kato Memorial Bioscience Foundation. Y.N. was supported by AMED the Research Program on Emerging and Re-emerging Infectious Diseases [21fk0108137h] and the JSPS KAKENHI [20KK0152]. H.T. and H.A. were funded by NOF CORPORATION as joint research.

Notes

The authors declare the following competing financial interest(s): H.T., Y.N., K.T., and H.A. are the inventors of a patent pending (WO2019/188867) on the ssPalm chemicals. This research was conducted as a joint research between Tohoku University, Chiba University, and the NOF CORPORATION.

ACKNOWLEDGMENTS

The authors wish to thank Dr. M. S. Feather for his helpful advice in writing the English manuscript. The authors would like to thank Ragab M. Fereig, Nanako Ushio, and Nanang R. Ariefta (National Research Center for Protozoan Diseases, Obihiro University of Agriculture and Veterinary Medicine) for their technical support with the mouse experiments, and Rumi Sato (RIKEN Center for Integrative Medical Sciences) for her technical assistance with histology of paraffin-embedded skin tissues. The authors express their gratitude to David Bzik (Dartmouth Medical School) for providing us with PruΔku80Δhxgprt parasites. The authors also thank Drs. K. Shimizu and S. Fujii on their help on breeding of zDC-DTR mice and Dr. M. Arita for discussion. BINDS is a framework governed by AMED to support collaboration among life

science researchers. This research was partially supported by Research Support Project for Life Science and Drug Discovery (Basis for Supporting Innovative Drug Discovery and Life Science Research (BINDS)) from AMED under Grant Number JP23ama121001.

REFERENCES

(1) Kim, J.; Eygeris, Y.; Gupta, M.; Sahay, G. Self-Assembled mRNA Vaccines. *Adv. Drug Delivery Rev.* **2021**, *170*, 83−112.
(2) Carvalho, T.; Krammer, F.; Iwasaki, A. The First 12 Months of Covid-19: A Timeline of Immunological Insights. *Nat. Rev. Immunol.* **2021**, *21*, 245−256.
(3) Ledford, H. Us Authorization of First Covid Vaccine Marks New Phase in Safety Monitoring. *Nature* **2020**, *588*, 377−378.
(4) Dolgin, E. The Tangled History of mRNA Vaccines. *Nature* **2021**, *597*, 318−324.
(5) Mullard, A. Pfizer's Covid-19 Vaccine Secures First Full FDA Approval. *Nat. Rev. Drug Discovery* **2021**, *20*, 728.
(6) Sahin, U.; Muik, A.; Derhovanessian, E.; Vogler, I.; Kranz, L. M.; Vormehr, M.; Baum, A.; Pascal, K.; Quandt, J.; Maurus, D.; Brachtendorf, S.; Lörks, V.; Sikorski, J.; Hilker, R.; Becker, D.; Eller, A. K.; Grützner, J.; Boesler, C.; Rosenbaum, C.; Kühnle, M. C.; et al. Covid-19 Vaccine BNT162b1 Elicits Human Antibody and T_H1 T Cell Responses. *Nature* **2020**, *586*, 594−599.
(7) Pulendran, B.; Arunachalam, P S.; O'Hagan, D. T. Emerging Concepts in the Science of Vaccine Adjuvants. *Nat. Rev. Drug Discovery* **2021**, *20*, 454−475.
(8) Russell, J. H.; Ley, T. J. Lymphocyte-Mediated Cytotoxicity. *Annu. Rev. Immunol.* **2002**, *20*, 323−370.
(9) Liu, G.; Zhu, M.; Zhao, X.; Nie, G. Nanotechnology-Empowered Vaccine Delivery for Enhancing CD8+ T Cells-Mediated Cellular Immunity. *Adv. Drug Delivery Rev.* **2021**, *176*, No. 113889.
(10) Jordan, K. A.; Hunter, C. A. Regulation of CD8+ T Cell Responses to Infection with Parasitic Protozoa. *Exp. Parasitol.* **2010**, *126*, 318−325.
(11) Wang, R.; Doolan, D. L.; Le, T. P.; Hedstrom, R. C.; Coonan, K. M.; Charoenvit, Y.; Jones, T. R.; Hobart, P.; Margalith, M.; Ng, J.; Weiss, W. R.; Sedegah, M.; de Taisne, C.; Norman, J. A.; Hoffman, S. L. Induction of Antigen-Specific Cytotoxic T Lymphocytes in Humans by a Malaria DNA Vaccine. *Science* **1998**, *282*, 476−480.
(12) Mallory, K. L.; Taylor, J. A.; Zou, X.; Waghela, I. N.; Schneider, C. G.; Sibilo, M. Q.; Punde, N. M.; Perazzo, L. C.; Savransky, T.; Sedegah, M.; Dutta, S.; Janse, C. J.; Pardi, N.; Lin, P. J. C.; Tam, Y. K.; Weissman, D.; Angov, E. Messenger RNA Expressing PfCSP Induces Functional, Protective Immune Responses against Malaria in Mice. *npj Vaccines* **2021**, *6*, 84.
(13) Tumeh, P. C.; Harview, C. L.; Yearley, J. H.; Shintaku, I. P.; Taylor, E. J.; Robert, L.; Chmielowski, B.; Spasic, M.; Henry, G.; Ciobanu, V.; West, A. N.; Carmona, M.; Kivork, C.; Seja, E.; Cherry, G.; Gutierrez, A. J.; Grogan, T. R.; Mateus, C.; Tomasic, G.; Glaspy, J. A.; et al. PD-1 Blockade Induces Responses by Inhibiting Adaptive Immune Resistance. *Nature* **2014**, *515*, 568−571.
(14) Miao, L.; Zhang, Y.; Huang, L. mRNA Vaccine for Cancer Immunotherapy. *Mol. Cancer* **2021**, *20*, 41.
(15) Pardi, N.; Hogan, M. J.; Porter, F. W.; Weissman, D. mRNA Vaccines - a New Era in Vaccinology. *Nat. Rev. Drug Discovery* **2018**, *17*, 261−279.
(16) Türeci, Ö.; Vormehr, M.; Diken, M.; Kreiter, S.; Huber, C.; Sahin, U. Targeting the Heterogeneity of Cancer with Individualized Neoepitope Vaccines. *Clin. Cancer Res.* **2016**, *22*, 1885−1896.
(17) Sahin, U.; Derhovanessian, E.; Miller, M.; Kloke, B. P.; Simon, P.; Löwer, M.; Bukur, V.; Tadmor, A. D.; Luxemburger, U.; Schrörs, B.; Omokoko, T.; Vormehr, M.; Albrecht, C.; Paruzynski, A.; Kuhn, A. N.; Buck, J.; Heesch, S.; Schreeb, K. H.; Müller, F.; Ortseifer, I.; et al. Personalized RNA Mutanome Vaccines Mobilize Poly-Specific Therapeutic Immunity against Cancer. *Nature* **2017**, *547*, 222−226.
(18) Tanaka, H.; Sakurai, Y.; Anindita, J.; Akita, H. Development of Lipid-Like Materials for RNA Delivery Based on Intracellular Environment-Responsive Membrane Destabilization and Spontaneous Collapse. *Adv. Drug Delivery Rev.* **2020**, *154*−*155*, 210−226.
(19) Ndeupen, S.; Qin, Z.; Jacobsen, S.; Bouteau, A.; Estanbouli, H.; Igyártó, B. Z. The mRNA-LNP Platform's Lipid Nanoparticle Component Used in Preclinical Vaccine Studies Is Highly Inflammatory. *iScience* **2021**, *24*, No. 103479.
(20) Tahtinen, S.; Tong, A. J.; Himmels, P.; Oh, J.; Paler-Martinez, A.; Kim, L.; Wichner, S.; Oei, Y.; McCarron, M. J.; Freund, E. C.; Amir, Z. A.; de la Cruz, C. C.; Haley, B.; Blanchette, C.; Schartner, J. M.; Ye, W.; Yadav, M.; Sahin, U.; Delamarre, L.; Mellman, I. IL-1 and IL-1ra Are Key Regulators of the Inflammatory Response to RNA Vaccines. *Nat. Immunol.* **2022**, *23*, 532−542.
(21) Li, C.; Lee, A.; Grigoryan, L.; Arunachalam, P. S.; Scott, M. K. D.; Trisal, M.; Wimmers, F.; Sanyal, M.; Weidenbacher, P. A.; Feng, Y.; Adamska, J. Z.; Valore, E.; Wang, Y.; Verma, R.; Reis, N.; Dunham, D.; O'Hara, R.; Park, H.; Luo, W.; Gitlin, A. D.; et al. Mechanisms of Innate and Adaptive Immunity to the Pfizer-Biontech BNT162b2 Vaccine. *Nat. Immunol.* **2022**, *23*, 543−555.
(22) Alameh, M. G.; Tombácz, I.; Bettini, E.; Lederer, K.; Ndeupen, S.; Sittplangkoon, C.; Wilmore, J. R.; Gaudette, B. T.; Soliman, O. Y.; Pine, M.; Hicks, P.; Manzoni, T. B.; Knox, J. J.; Johnson, J. L.; Laczkó, D.; Muramatsu, H.; Davis, B.; Meng, W.; Rosenfeld, A. M.; Strohmeier, S.; Lin, P. J. C.; et al. Lipid Nanoparticles Enhance the Efficacy of mRNA and Protein Subunit Vaccines by Inducing Robust T Follicular Helper Cell and Humoral Responses. *Immunity* **2021**, *54*, 2877−2892.e2877.
(23) Miao, L.; Li, L.; Huang, Y.; Delcassian, D.; Chahal, J.; Han, J.; Shi, Y.; Sadtler, K.; Gao, W.; Lin, J.; Doloff, J. C.; Langer, R.; Anderson, D. G. Delivery of mRNA Vaccines with Heterocyclic Lipids Increases Anti-Tumor Efficacy by Sting-Mediated Immune Cell Activation. *Nat. Biotechnol.* **2019**, *37*, 1174−1185.
(24) Tanaka, H.; Akita, H.; Ishiba, R.; Tange, K.; Arai, M.; Kubo, K.; Harashima, H. Neutral Biodegradable Lipid-Envelope-Type Nanoparticle Using Vitamin A-Scaffold for Nuclear Targeting of Plasmid DNA. *Biomaterials* **2014**, *35*, 1755−1761.
(25) Tanaka, H.; Watanabe, A.; Konishi, M.; Nakai, Y.; Yoshioka, H.; Ohkawara, T.; Takeda, H.; Harashima, H.; Akita, H. The Delivery of mRNA to Colon Inflammatory Lesions by Lipid-Nano-Particles Containing Environmentally-Sensitive Lipid-Like Materials with Oleic Acid Scaffolds. *Heliyon* **2018**, *4*, No. e00959.
(26) Kawai, M.; Nakamura, T.; Miura, N.; Maeta, M.; Tanaka, H.; Ueda, K.; Higashi, K.; Moribe, K.; Tange, K.; Nakai, Y.; Yoshioka, H.; Harashima, H.; Akita, H. DNA-Loaded Nano-Adjuvant Formed with a Vitamin E-Scaffold Intracellular Environmentally-Responsive Lipid-Like Material for Cancer Immunotherapy. *Nanomedicine: nanotechnology, biology, and medicine* **2018**, *14*, 2587−2597.
(27) Maeta, M.; Miura, N.; Tanaka, H.; Nakamura, T.; Kawanishi, R.; Nishikawa, Y.; Asano, K.; Tanaka, M.; Tamagawa, S.; Nakai, Y.; Tange, K.; Yoshioka, H.; Harashima, H.; Akita, H. Vitamin E Scaffolds of pH-Responsive Lipid Nanoparticles as DNA Vaccines in Cancer and Protozoan Infection. *Mol. Pharmaceutics* **2020**, *17*, 1237−1247.
(28) Tateshita, N.; Miura, N.; Tanaka, H.; Masuda, T.; Ohtsuki, S.; Tange, K.; Nakai, Y.; Yoshioka, H.; Akita, H. Development of a Lipoplex-Type mRNA Carrier Composed of an Ionizable Lipid with a Vitamin E Scaffold and the KALA Peptide for Use as an Ex Vivo Dendritic Cell-Based Cancer Vaccine. *J. Controlled Release* **2019**, *310*, 36−46.
(29) Akita, H.; Ishiba, R.; Hatakeyama, H.; Tanaka, H.; Sato, Y.; Tange, K.; Arai, M.; Kubo, K.; Harashima, H. A Neutral Envelope-Type Nanoparticle Containing pH-Responsive and SS-Cleavable Lipid-Like Material as a Carrier for Plasmid DNA. *Adv. Healthcare Mater.* **2013**, *2*, 1120−1125.
(30) Akita, H.; Noguchi, Y.; Hatakeyama, H.; Sato, Y.; Tange, K.; Nakai, Y.; Harashima, H. Molecular Tuning of a Vitamin E-Scaffold pH-Sensitive and Reductive Cleavage Lipid-Like Material for Accelerated in Vivo Hepatic siRNA Delivery. *ACS Biomater. Sci. Eng.* **2015**, *1*, 834−844.
(31) Bettinger, T.; Carlisle, R. C.; Read, M. L.; Ogris, M.; Seymour, L. W. Peptide-Mediated RNA Delivery: A Novel Approach for

https://doi.org/10.1021/acsnano.3c02251
ACS Nano 2023, 17, 18758−18774

Enhanced Transfection of Primary and Post-Mitotic Cells. *Nucleic Acids Res.* **2001**, *29*, 3882−3891.
(32) Kimura, N.; Maeki, M.; Sato, Y.; Note, Y.; Ishida, A.; Tani, H.; Harashima, H.; Tokeshi, M. Development of the iLiNP Device: Fine Tuning the Lipid Nanoparticle Size within 10 nm for Drug Delivery. *ACS Omega* **2018**, *3*, 5044−5051.
(33) Hassett, K. J.; Higgins, J.; Woods, A.; Levy, B.; Xia, Y.; Hsiao, C. J.; Acosta, E.; Almarsson, Ö.; Moore, M. J.; Brito, L. A. Impact of Lipid Nanoparticle Size on mRNA Vaccine Immunogenicity. *J. Controlled Release* **2021**, *335*, 237−246.
(34) Brader, M. L.; Williams, S. J.; Banks, J. M.; Hui, W. H.; Zhou, Z. H.; Jin, L. Encapsulation State of Messenger RNA inside Lipid Nanoparticles. *Biophys. J.* **2021**, *120*, 2766−2770.
(35) De Beuckelaer, A.; Pollard, C.; Van Lint, S.; Roose, K.; Van Hoecke, L.; Naessens, T.; Udhayakumar, V. K.; Smet, M.; Sanders, N.; Lienenklaus, S.; Saelens, X.; Weiss, S.; Vanham, G.; Grooten, J.; De Koker, S. Type I Interferons Interfere with the Capacity of mRNA Lipoplex Vaccines to Elicit Cytolytic T Cell Responses. *Mol. Ther.* **2016**, *24*, 2012−2020.
(36) Eisenbarth, S. C. Dendritic Cell Subsets in T Cell Programming: Location Dictates Function. *Nat. Rev. Immunol.* **2019**, *19*, 89−103.
(37) Kitano, M.; Yamazaki, C.; Takumi, A.; Ikeno, T.; Hemmi, H.; Takahashi, N.; Shimizu, K.; Fraser, S. E.; Hoshino, K.; Kaisho, T.; Okada, T. Imaging of the Cross-Presenting Dendritic Cell Subsets in the Skin-Draining Lymph Node. *Proc. Natl. Acad. Sci. U. S. A.* **2016**, *113*, 1044−1049.
(38) Yamazaki, C.; Sugiyama, M.; Ohta, T.; Hemmi, H.; Hamada, E.; Sasaki, I.; Fukuda, Y.; Yano, T.; Nobuoka, M.; Hirashima, T.; Iizuka, A.; Sato, K.; Tanaka, T.; Hoshino, K.; Kaisho, T. Critical Roles of a Dendritic Cell Subset Expressing a Chemokine Receptor, XCR1. *J. Immunol.* **2013**, *190*, 6071−6082.
(39) Madisen, L.; Zwingman, T. A.; Sunkin, S. M.; Oh, S. W.; Zariwala, H. A.; Gu, H.; Ng, L. L.; Palmiter, R. D.; Hawrylycz, M. J.; Jones, A. R.; Lein, E. S.; Zeng, H. A Robust and High-Throughput Cre Reporting and Characterization System for the Whole Mouse Brain. *Nat. Neurosci.* **2010**, *13*, 133−140.
(40) Idoyaga, J.; Fiorese, C.; Zbytnuik, L.; Lubkin, A.; Miller, J.; Malissen, B.; Mucida, D.; Merad, M.; Steinman, R. M. Specialized Role of Migratory Dendritic Cells in Peripheral Tolerance Induction. *J. Clin. Invest.* **2013**, *123*, 844−854.
(41) Coffman, R. L.; Sher, A.; Seder, R. A. Vaccine Adjuvants: Putting Innate Immunity to Work. *Immunity* **2010**, *33*, 492−503.
(42) Alexopoulou, L.; Holt, A. C.; Medzhitov, R.; Flavell, R. A. Recognition of Double-Stranded RNA and Activation of NF-KappaB by Toll-Like Receptor 3. *Nature* **2001**, *413*, 732−738.
(43) Trumpfheller, C.; Caskey, M.; Nchinda, G.; Longhi, M. P.; Mizenina, O.; Huang, Y.; Schlesinger, S. J.; Colonna, M.; Steinman, R. M. The Microbial Mimic Poly IC Induces Durable and Protective CD4+ T Cell Immunity Together with a Dendritic Cell Targeted Vaccine. *Proc. Natl. Acad. Sci. U. S. A.* **2008**, *105*, 2574−2579.
(44) Longhi, M. P.; Trumpfheller, C.; Idoyaga, J.; Caskey, M.; Matos, I.; Kluger, C.; Salazar, A. M.; Colonna, M.; Steinman, R. M. Dendritic Cells Require a Systemic Type I Interferon Response to Mature and Induce CD4+ Th1 Immunity with Poly IC as Adjuvant. *J. Exp. Med.* **2009**, *206*, 1589−1602.
(45) Desmet, C. J.; Ishii, K. J. Nucleic Acid Sensing at the Interface between Innate and Adaptive Immunity in Vaccination. *Nat. Rev. Immunol.* **2012**, *12*, 479−491.
(46) Kranz, L. M.; Diken, M.; Haas, H.; Kreiter, S.; Loquai, C.; Reuter, K. C.; Meng, M.; Fritz, D.; Vascotto, F.; Hefesha, H.; Grunwitz, C.; Vormehr, M.; Hüsemann, Y.; Selmi, A.; Kuhn, A. N.; Buck, J.; Derhovanessian, E.; Rae, R.; Attig, S.; Diekmann, J.; et al. Systemic RNA Delivery to Dendritic Cells Exploits Antiviral Defence for Cancer Immunotherapy. *Nature* **2016**, *534*, 396−401.
(47) Akira, S.; Takeda, K.; Kaisho, T. Toll-Like Receptors: Critical Proteins Linking Innate and Acquired Immunity. *Nat. Immunol.* **2001**, *2*, 675−680.
(48) Davies, N.; Hovdal, D.; Edmunds, N.; Nordberg, P.; Dahlén, A.; Dabkowska, A.; Arteta, M. Y.; Radulescu, A.; Kjellman, T.; Höijer, A.; Seeliger, F.; Holmedal, E.; Andihn, E.; Bergenhem, N.; Sandinge, A. S.; Johansson, C.; Hultin, L.; Johansson, M.; Lindqvist, J.; Björsson, L.; et al. Functionalized Lipid Nanoparticles for Subcutaneous Administration of mRNA to Achieve Systemic Exposures of a Therapeutic Protein. *Mol. Ther.–Nucleic Acids* **2021**, *24*, 369−384.
(49) Akinc, A.; Maier, M. A.; Manoharan, M.; Fitzgerald, K.; Jayaraman, M.; Barros, S.; Ansell, S.; Du, X.; Hope, M. J.; Madden, T. D.; Mui, B. L.; Semple, S. C.; Tam, Y. K.; Ciufolini, M.; Witzigmann, D.; Kulkarni, J. A.; van der Meel, R.; Cullis, P. R. The Onpattro Story and the Clinical Translation of Nanomedicines Containing Nucleic Acid-Based Drugs. *Nat. Nanotechnol.* **2019**, *14*, 1084−1087.
(50) Crotty, S. T Follicular Helper Cell Differentiation, Function, and Roles in Disease. *Immunity* **2014**, *41*, 529−542.
(51) Verbeke, R.; Hogan, M. J.; Loré, K.; Pardi, N. Innate Immune Mechanisms of mRNA Vaccines. *Immunity* **2022**, *55*, 1993−2005.
(52) Montoya, M.; Schiavoni, G.; Mattei, F.; Gresser, I.; Belardelli, F.; Borrow, P.; Tough, D. F. Type I Interferons Produced by Dendritic Cells Promote Their Phenotypic and Functional Activation. *Blood* **2002**, *99*, 3263−3271.
(53) Curtsinger, J. M.; Valenzuela, J. O.; Agarwal, P.; Lins, D.; Mescher, M. F. Type I IFNs Provide a Third Signal to CD8 T Cells to Stimulate Clonal Expansion and Differentiation. *J. Immunol.* **2005**, *174*, 4465−4469.
(54) Kolumam, G. A.; Thomas, S.; Thompson, L. J.; Sprent, J.; Murali-Krishna, K. Type I Interferons Act Directly on CD8 T Cells to Allow Clonal Expansion and Memory Formation in Response to Viral Infection. *J. Exp. Med.* **2005**, *202*, 637−650.
(55) King, C.; Sprent, J. Dual Nature of Type I Interferons in SARS-Cov-2-Induced Inflammation. *Trends Immunol.* **2021**, *42*, 312−322.
(56) Duong, E.; Fessenden, T. B.; Lutz, E.; Dinter, T.; Yim, L.; Blatt, S.; Bhutkar, A.; Wittrup, K. D.; Spranger, S. Type I Interferon Activates MHC Class I-Dressed $CD11b^{+}$ Conventional Dendritic Cells to Promote Protective Anti-Tumor $CD8^{+}$ T cell Immunity. *Immunity* **2022**, *55*, 308−323.e309.
(57) Ivashkiv, L. B.; Donlin, L. T. Regulation of Type I Interferon Responses. *Nat. Rev. Immunol.* **2014**, *14*, 36−49.
(58) Cohet, C.; van der Most, R.; Bauchau, V.; Bekkat-Berkani, R.; Doherty, T. M.; Schuind, A.; Tavares Da Silva, F.; Rappuoli, R.; Garçon, N.; Innis, B. L. Safety of AS03-Adjuvanted Influenza Vaccines: A Review of the Evidence. *Vaccine* **2019**, *37*, 3006−3021.
(59) Morel, S.; Didierlaurent, A.; Bourguignon, P.; Delhaye, S.; Baras, B.; Jacob, V.; Planty, C.; Elouahabi, A.; Harvengt, P.; Carlsen, H.; Kielland, A.; Chomez, P.; Garçon, N.; Van Mechelen, M. Adjuvant System AS03 Containing α-Tocopherol Modulates Innate Immune Response and Leads to Improved Adaptive Immunity. *Vaccine* **2011**, *29*, 2461−2473.
(60) Gong, T.; Liu, L.; Jiang, W.; Zhou, R. DAMP-Sensing Receptors in Sterile Inflammation and Inflammatory Diseases. *Nat. Rev. Immunol.* **2020**, *20*, 95−112.
(61) Onishi, M.; Ozasa, K.; Kobiyama, K.; Ohata, K.; Kitano, M.; Taniguchi, K.; Homma, T.; Kobayashi, M.; Sato, A.; Katakai, Y.; Yasutomi, Y.; Wijaya, E.; Igarashi, Y.; Nakatsu, N.; Ise, W.; Inoue, T.; Yamada, H.; Vandenbon, A.; Standley, D. M.; Kurosaki, T.; et al. Hydroxypropyl-B-Cyclodextrin Spikes Local Inflammation That Induces Th2 Cell and T Follicular Helper Cell Responses to the Coadministered Antigen. *J. Immunol.* **2015**, *194*, 2673−2682.
(62) Embgenbroich, M.; Burgdorf, S. Current Concepts of Antigen Cross-Presentation. *Front. Immunol.* **2018**, *9*, 1643.
(63) Liu, M. A. Immunologic Basis of Vaccine Vectors. *Immunity* **2010**, *33*, 504−515.
(64) Neefjes, J.; Jongsma, M. L.; Paul, P.; Bakke, O. Towards a Systems Understanding of MHC Class I and MHC Class II Antigen Presentation. *Nat. Rev. Immunol.* **2011**, *11*, 823−836.
(65) Eickhoff, S.; Brewitz, A.; Gerner, M. Y.; Klauschen, F.; Komander, K.; Hemmi, H.; Garbi, N.; Kaisho, T.; Germain, R. N.; Kastenmüller, W. Robust Anti-Viral Immunity Requires Multiple

https://doi.org/10.1021/acsnano.3c02251
ACS Nano 2023, 17, 18758−18774

Distinct T Cell-Dendritic Cell Interactions. *Cell* **2015**, *162*, 1322−1337.
(66) Savina, A.; Jancic, C.; Hugues, S.; Guermonprez, P.; Vargas, P.; Moura, I. C.; Lennon-Duménil, A. M.; Seabra, M. C.; Raposo, G.; Amigorena, S. NOX2 Controls Phagosomal pH to Regulate Antigen Processing During Crosspresentation by Dendritic Cells. *Cell* **2006**, *126*, 205−218.
(67) Miura, N.; Shaheen, S. M.; Akita, H.; Nakamura, T.; Harashima, H. A KALA-Modified Lipid Nanoparticle Containing CpG-Free Plasmid DNA as a Potential DNA Vaccine Carrier for Antigen Presentation and as an Immune-Stimulative Adjuvant. *Nucleic Acids Res.* **2015**, *43*, 1317−1331.
(68) Soneson, C.; Love, M. I.; Robinson, M. D. Differential Analyses for RNA-Seq: Transcript-Level Estimates Improve Gene-Level Inferences. *F1000Research* **2015**, *4*, 1521.
(69) Ge, S. X.; Son, E. W.; Yao, R. iDEP: An Integrated Web Application for Differential Expression and Pathway Analysis of RNA-Seq Data. *BMC Bioinf.* **2018**, *19*, 534.
(70) Laurens van der Maaten, G. H. Visualizing Data Using t-SNE. *J. Mach Learn Res.* **2008**, *9*, 27.
(71) Love, M. I.; Huber, W.; Anders, S. Moderated Estimation of Fold Change and Dispersion for RNA-Seq Data with DESeq2. *Genome Biol.* **2014**, *15*, 550.
(72) Luo, W.; Friedman, M. S.; Shedden, K.; Hankenson, K. D.; Woolf, P. J. Gage: Generally Applicable Gene Set Enrichment for Pathway Analysis. *BMC Bioinf.* **2009**, *10*, 161.

https://doi.org/10.1021/acsnano.3c02251
ACS Nano 2023, 17, 18758−18774